Bachelorarbeit

On the Isotropic Distorted Structure of Colloidal Dispersions Under Shear

Alexander Blech

vorgelegt am 4. August 2015

am Fachbereich Physik der

1. Gutachter: Professor Dr. M. Fuchs
2. Gutachter: Dr. M. Krüger

Überarbeitete Version vom 10.01.2016

Zusammenfassung

In einem ersten Schritt wird der theoretische Rahmen zur Beschreibung der nichtlinearen rheologischen Eigenschaften in dichten Kolloid-Dispersionen unter konstanter Scherung präsentiert, beginnend mit dem Wechselspiel zwischen Brown'scher Bewegung und speziell durch Scherung hervorgerufenen dynamischen Eigenschaften. Im weiteren Verlauf ergibt sich eine in sich geschlossene Moden-Kopplungs-Theorie mit exakten nichtlinearen Green-Kubo-Relationen, wodurch beliebige stationäre Mittelwerte durch Integration über den nicht-stationären Bereich berechnet werden können. Näherungen im Rahmen dieser Theorie verknüpfen, mithilfe der transienten Dichtekorrelationsfunktionen, diese Mittelwerte mit der nichtstationären Dynamik. Vor diesem Hintergrund wird die Struktur einer Dispersion mit angelegter Scherung, in Form einer Störung, numerisch berechnet, wobei der isotrope Anteil explizit berücksichtig wird, der in vorherigen Untersuchungen vernachlässigt wurde. Obwohl dieser die tranversale Spannung nicht beeinflusst, beeinflusst er die makroskopischen normalen Spannungskomponenten stark und ändert das Vorzeichen des deviatorischen Drucks. Zudem hängen die Kontaktwerte der lokalen Paarkorrelationsfunktionen stark vom isotropen Anteil ab, die mit diesen Korrekturen besser mit der Simulation der Brown'schen Dynamik von [Ama+15] übereinstimmen.

Abstract

The theoretical background for non-linear rheological properties of dense colloidal dispersions under steady shear are presented, starting from the microscopic competition between Brownian motion and shear induced dynamics. From this point of view the steady state properties are approached by the integration through transients, resulting in a closed mode coupling theory, which contains exact non-linear Green-Kubo relations for arbitrary stationary expectation values. It is shown how approximations motivated by MCT connect this averages with the transient dynamics using the transient density correlation functions. On this background the distorted structure under shear was calculated numerically, taking explicitly account for the isotropic contribution, which was neglected in former calculations. Albeit they does not affect the transverse stress, it could be found that these causes major qualitative differences on the macroscopic normal stress components and provides a correction of the sign of the deviatoric pressure. At last this is connected to the contact values of the local pair correlations, which this corrections leads to more agreement with data obtained by Brownian dynamic simulations from [Ama+15].

Contents

1. Introduction

Structure functions and time dependent correlation functions far from thermal equilibrium are important topics in non-linear rheology. Since colloidal dispersions under shear can easily be investigated, e.g. by confocal microscopy, they are model systems for much more complicated systems and even for the atomic scale. The mode coupling theory (MCT) provides an efficient theoretical framework, connecting Brownian dynamics with shear-induced rearrangements - while hydrodynamic interactions (HI) are neglected - which will be presented in the first part of this elaboration, in order to approach the stationary properties of stress and structural relaxation in a dense dispersion under steady shear. The integration through transients approach (ITT) connects steady state averages with the transient dynamics in the system, which are encoded in density correlation functions. By integrating this transient response from the system of the shear-induced dynamics, the distortion of the stationary non-equilibrium structure factor is obtainable. This structural distortion was calculated numerically and discussed with respect to its effects on the transversal and normal stress tensor components. Albeit MCT-ITT shows good agreement with simulation data of the quadrupolar and hexadecopular deformation modes of the local pair order ([Ama+15]), the isotropic contributions are not captured by the theory. Hence especially the isotropic structural distortion and its effect on the deviatoric pressure is discussed in this elaboration.

2. Microscopic Starting Point

2.1. Colloidal Particles under Shear

The considered system shall consist of N spherical colloidal particles of diameter d dispersed in a volume V of a solvent with viscosity η_s. $\Psi(\Gamma, t)$ shall denote the distribution function of the particle's positions $\boldsymbol{r}_i$ at time t, which are combined in $\Gamma = \{\boldsymbol{r}_i\}$ (with $i \in \{1, \ldots, N\}$) abbreviating the full set of particle positions. For time $t_0 = 0$ the system is assumed to be in an equilibrium state of temperature T where the distribution function is called $\Psi_\mathrm{e} = \Psi(\Gamma, t_0)$. For times $t > t_0$ homogeneous shear is imposed with shear rate tensor $\boldsymbol{\kappa} = \dot{\gamma}\hat{\boldsymbol{x}}\hat{\boldsymbol{y}}$ (whereupon $\hat{\boldsymbol{x}}$,$\hat{\boldsymbol{y}}$ denote the canonic unit vectors in the appropriate direction). The velocity of the corresponding flow profile $\boldsymbol{v}(\boldsymbol{r}) = \boldsymbol{\kappa}\boldsymbol{r}$ points along the x-axis and its gradient along the y-axis. The unit convention [length] $= d$, [energy] $= k_\mathrm{B}T$ and [time] $= d^2/D_0$ with the bare diffusion coefficient D_0 of a single particle leads to dimensionless quantities.

The dynamic of this system arises from interactions between the colloidal particles and interactions of the particles with the solvent. While the first are given by interparticle forces $\boldsymbol{F}_i = -\boldsymbol{\partial}_i U(\{\boldsymbol{r}_i\})$ deriving from the total potential energy U, the latter are composed of hydrodynamic interactions (HI), solvent friction measured by the Stokes friction coefficient $\zeta = 6\pi\eta_\mathrm{s}d$ and random kicks from the solvent. While the HI are neglected in this approach the latter is implemented via a noise function. This leads to a set of N coupled Langevin equations describing the motion of the particles [Fuc10]:

$$\zeta\left(\frac{\mathrm{d}\boldsymbol{r}_i}{\mathrm{d}t} - \boldsymbol{v}(\boldsymbol{r}_i)\right) = \boldsymbol{F}_i + \boldsymbol{f}_i \ . \tag{2.1}$$

The friction part on the left is proportional to the particle's velocity compared to the solvent's flow. The noise force $\boldsymbol{f}_i$ experienced by the ith particle can be assumed to be of white Gaussian type and satisfies

$$\langle f_i^\alpha(t) f_j^\beta(t')\rangle = 2\zeta\delta_{\alpha\beta}\delta_{ij}\delta(t - t') \tag{2.2}$$

where α, β denote directions [Fuc10]. The fluctuation dissipation theorem also holds for the random force giving the Einstein-Smoluchowski relation $D_0 = k_\mathrm{B}T/\zeta$. On average, friction and interparticle forces cancel one another for each particle, giving the affine motion $\langle \boldsymbol{r}_i(t)\rangle = \boldsymbol{r}_i(0) + \dot{\gamma}t y_i(0)\hat{\boldsymbol{x}}$, because these balances result in an average resting of the particles relative to the solvent. For $\boldsymbol{F}_i = 0$ equation (2.1)

captures the effect of a Taylor dispersion leading to a super-diffusive behaviour [Fuc10].

As mentioned before, the system starts in the equilibrium state with probability distribution Ψ_e, which is of the Boltzmann-Gibbs type [FC09],[Fuc10]. Although the dynamics in (2.1) may drive the system far away from equilibrium, the assumption can be made that the system finally relaxes in a stationary state with a distribution function $\Psi(t \to \infty) = \Psi_\mathrm{s}$. This assumption is self consistent in MCT-ITT, because it also is a prediction for all systems under shear [Fuc10]. To describe the temporal evolution of $\Psi(\Gamma, t)$ it is possible to reformulate (2.1) as a conservation law for the probability distribution, which is called the Smoluchowski equation [Fuc10]:

$$\partial_t \Psi + \nabla \cdot \boldsymbol{j} = \partial_t \Psi + \sum_{i=1}^{N} \boldsymbol{\partial}_i \cdot \boldsymbol{j}_i = 0 \tag{2.3}$$

with a probability flux

$$\boldsymbol{j}_i = D_0 \left[-\boldsymbol{\partial}_i + \boldsymbol{F}_i + \dot{\gamma} y_i \hat{\boldsymbol{x}} \right] \Psi \tag{2.4}$$

(in the following summation indices capture their hole range if not marked explicitly). Both the equilibrium and the stationary state are time-independent and their distribution functions therefore satisfy $\partial_t \Psi_\mathrm{s} = 0$ (and $\partial_t \Psi_\mathrm{e} = 0$ without shear). But the non-zero curl of the friction force in (2.1) induces a non-zero stationary probability flux $\boldsymbol{j}_i^\mathrm{s} \neq 0$. Hence, the stationary distribution function Ψ_s cannot be of equilibrium Boltzmann-Gibbs type [Fuc10]. For further progress it is convenient to define the Smoluchowski operator (SO) Ω by reformulating (2.3) as

$$\partial_t \Psi(\Gamma, t) = \Omega(\Gamma) \Psi(\Gamma, t) \tag{2.5}$$

[FC09] with

$$\Omega \equiv \sum_i \boldsymbol{\partial}_i \cdot \left(\boldsymbol{\partial}_i - \boldsymbol{F}_i - \boldsymbol{\kappa} \cdot \boldsymbol{r}_i \right) . \tag{2.6}$$

The SO can be divided into $\Omega = \Omega_\mathrm{e} + \delta\Omega$ whereupon $\Omega_\mathrm{e} = \boldsymbol{\partial}_i \cdot (\boldsymbol{\partial}_i \boldsymbol{F}_i)$ denotes the SO without shear and $\delta\Omega$ can be seen as shear-induced perturbation [FC09]. The former has a zero eigenvalue whose eigenfunction is the equilibrium distribution Ψ_e. The stationary non-equilibrium distribution Ψ_s plays this role for the full SO [FC09], viz. they are characterised by

$$\Omega_\mathrm{e} \Psi_\mathrm{e} = 0, \qquad \Omega \Psi_\mathrm{s} = 0 . \tag{2.7}$$

The Smoluchowski equation (2.5) has a form similar to the time dependent Schrödinger equation in quantum physics where the SO replaces the Hamilton operator. With respect to equilibrium averaging, Ψ_e is even an hermitian operator [FC09] but with applied shear, particle fluxes in the steady state violate time reversal symmetry

and therefore the detailed balance principle; thus it is impossible to shape the SO to satisfy $\Omega = \Omega^\dagger$ [FC09]. However, in MCT the adjoint SO $\Omega^\dagger$ proofs crucial and can be developed using the incompressibility condition Trace $\boldsymbol{\kappa} = 0$ and partial integration [FC09]:

$$\Omega^\dagger = \sum_i (\boldsymbol{\partial}_i + \boldsymbol{F}_i + \boldsymbol{r}_i \cdot \boldsymbol{\kappa}^T) \cdot \boldsymbol{\partial}_i \; . \tag{2.8}$$

Similar to the transformation of the Schrödinger representation into a Heisenberg representation, this step enables acting with the adjoint operator on quantities to be averaged with Ψ_s, rather than acting on the probability distributions themselves. Thus, relations can be obtained of averages being taken with the stationary distributions wherefore closure approximations are much easier to apply [FC09]. The adjoint SO can also be divided into $\Omega^\dagger = \Omega^\dagger_\mathrm{e} + \delta\Omega^\dagger$ whereupon the perturbation fulfils

$$\delta\Omega^\dagger = \sum_i \boldsymbol{\partial}_i \cdot \boldsymbol{\kappa} \cdot \boldsymbol{r}_i = \sum_i \boldsymbol{r}_i \cdot \boldsymbol{\kappa}^T \cdot \boldsymbol{\partial}_i \; . \tag{2.9}$$

At this point the potential part of the macroscopic stress tensor can enter the approach in an active way. It arises from the inner forces between the particles in the following form

$$\sigma_{\alpha\beta} = -\sum_i \boldsymbol{F}_i^\alpha \boldsymbol{r}_i^\beta \tag{2.10}$$

and can be used to express the perturbation of the SO:

$$\begin{aligned} \delta\Omega\Psi_\mathrm{e} &= -\sum_i \boldsymbol{\partial}_i \cdot \boldsymbol{\kappa} \cdot \boldsymbol{r}_i \Psi_\mathrm{e} = -\sum_i \boldsymbol{F}_i \cdot \boldsymbol{\kappa} \cdot \boldsymbol{r}_i \Psi_\mathrm{e} \\ &= \mathrm{Trace}\,(\boldsymbol{\kappa} \cdot \boldsymbol{\sigma})\, \Psi_\mathrm{e} = \dot\gamma \sigma_{xy} \Psi_\mathrm{e} \; . \end{aligned} \tag{2.11}$$

This shows that the stress tensor provides the transition between equilibrium and non-equilibrium averages, with the shear stress acting as the generator of this transformation. This will be found later, leading to a connection between steady state properties and the transient shear-depending dynamics, which is the quintessence of the ITT approach [Fuc10],[FC09].

2.2. Exploiting Translational Invariance

As mentioned in the beginning the system is considered to be homogeneous and amorphous, hence the equilibrium probability density Ψ_e is translational invariant. Although shear flow breaks rotational and translational invariance of the SO, the stationary distribution Ψ_s remains translational invariant as showed in [Fuc10]. To

take account of this invariance property it is useful to transform into Fourier space and have a look at steady state quantities of wavevector-dependent fluctuations

$$f_{\boldsymbol{q}}(\Gamma,t) \equiv e^{\Omega^\dagger t}\sum_j X_j^f(\Gamma)e^{i\boldsymbol{q}\cdot\boldsymbol{r}_j} \tag{2.12}$$

where f (and also g in the following) denotes an arbitrary function of all particle positions. Note, that $f_{\boldsymbol{q}}(\Gamma,t)$ is also depending on the shear rate $\dot\gamma$, which is concealed in the adjoint SO. The exponential function with the adjoint SO acts as a time evolution operator, driving a fluctuation that occurred in the initial equilibrium state to a time t after switch-on of the shear [Fuc10],[FC09]. The density Fourier components $f_{\boldsymbol{q}}(\Gamma,t)=\rho_{\boldsymbol{q}}(t)$ can be obtained from X_i^ρ, whereas $X_i^{\boldsymbol{\sigma}}$ leads to the full wavevector-dependent stress tensor $f_{\boldsymbol{q}}(\Gamma,t)=\sigma_{\alpha\beta}(\boldsymbol{q},\Gamma(t))$:

$$X_i^\rho = 1\ , \tag{2.13}$$

$$X_i^{\sigma_{\alpha\beta}} = \delta_{\alpha\beta} + \frac{1}{2}\sum_{j\neq i}(r_i^\alpha - r_j^\alpha)\frac{\mathrm{d}u(|\boldsymbol{r}_i-\boldsymbol{r}_j|)}{\mathrm{d}r_i^\beta}\ . \tag{2.14}$$

Here $u(|\boldsymbol{r}_i-\boldsymbol{r}_j|)$ denotes the pair potential of the particles i and j.

Translational invariance means that averages of quantities depending on particle positions must be independent of identical shifts of all particle positions $\Gamma\to\Gamma'$ with $\boldsymbol{r}_i'=\boldsymbol{r}_i+\boldsymbol{a}$. Since under this shift the SO becomes [Fuc10],[FC09]

$$\Omega^\dagger(\Gamma) = \Omega^\dagger(\Gamma') - \boldsymbol{P}\cdot\boldsymbol{\kappa}\cdot\boldsymbol{a}, \qquad \text{with} \quad \boldsymbol{P}=\sum_i \boldsymbol{\partial}_i\ , \tag{2.15}$$

for fluctuations that depend on particle separations only follows:

$$f_{\boldsymbol{q}}(\Gamma,t) = e^{-i(\boldsymbol{q}+\boldsymbol{q}\cdot\kappa t)\cdot\boldsymbol{a}} f_{\boldsymbol{q}}(\Gamma',t)\ . \tag{2.16}$$

Thus, and because phase space integrals must match for both integration variables Γ,Γ'

$$\int \mathrm{d}\Gamma\Psi(\Gamma)f_{\boldsymbol{q}}(\Gamma) \stackrel{!}{=} \int \mathrm{d}\Gamma'\Psi(\Gamma')f_{\boldsymbol{q}}(\Gamma')e^{-i(\boldsymbol{q}+\boldsymbol{q}\boldsymbol{\kappa})\boldsymbol{a}} \tag{2.17}$$

steady state averages vanish except for zero wavevector [Fuc10],[FC09]:

$$\frac{1}{V}\langle f_{\boldsymbol{q}}(t)\rangle^{(\dot\gamma)} = f_0(\dot\gamma)\delta_{q,0} \equiv f(\dot\gamma)\ . \tag{2.18}$$

Here and in the following $\langle\ldots\rangle^{(\dot\gamma)}\equiv\int\ldots\Phi_\mathrm{s}(\Gamma)\mathrm{d}\Gamma$ shall denote a stationary average, whereas equilibrium averages are abbreviated with $\langle\ldots\rangle\equiv\int\ldots\Phi_\mathrm{e}(\Gamma)\mathrm{d}\Gamma$.

Similarly argued equal time correlators built from pairs of fluctuations $\delta f_{\boldsymbol{q}},\delta g_{\boldsymbol{q}'}$ are diagonal in $\boldsymbol{q},\boldsymbol{q}'$. Thus, it is sufficient to introduce these as structure functions of f,g using a single wavevector only [FC09]:

$$S_{fg;\boldsymbol{q}}(\dot\gamma) \equiv \frac{1}{N}\langle\delta f_{\boldsymbol{q}}^*\delta g_{\boldsymbol{q}}\rangle^{(\dot\gamma)}\ . \tag{2.19}$$

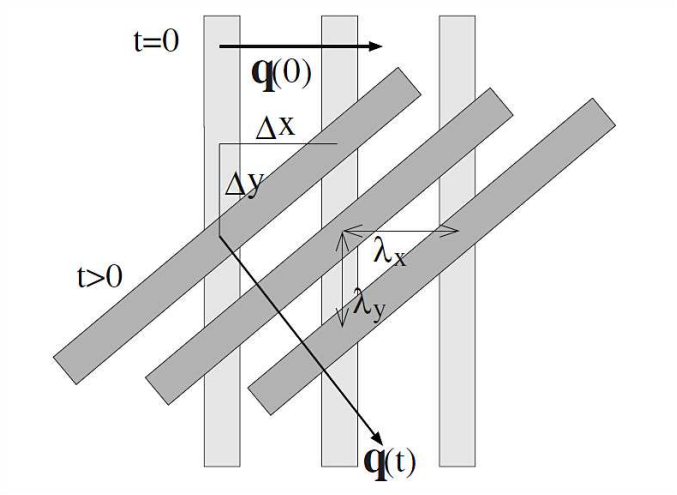

Figure 2.1.: Shear advection of a fluctuation with initial wavevector in x-direction, $\boldsymbol{q}(t_0 = 0) = q(1, 0, 0)^{\mathrm{T}}$ and advected wavevector at later time $\boldsymbol{q}(t > t_0) = q(1, -\dot{\gamma}t, 0)^{\mathrm{T}}$; from [FC09]. While λ_x is the wavelength in x-direction at t_0, at later time t the corresponding wavelength λ_y in (negative) y-direction obeys $\lambda_x/\lambda_y = \Delta x/\Delta y = \dot{\gamma}t$. At all times, $\boldsymbol{q}(t)$ is perpendicular to the planes of constant fluctuation amplitude. Note that the magnitude $q(t) = q\sqrt{1 + (\dot{\gamma}t)^2}$ increases with time. Brownian motion, neglected in this sketch, would smear out the fluctuation.

The symbol $\delta X \equiv X - \langle X \rangle^{(\dot{\gamma})}$ stands for a fluctuation of X around the stationary state, while later $\Delta X \equiv X - \langle X \rangle$ will denote fluctuations around the equilibrium. If not marked explicitly the suppressed time argument of the fluctuations is arbitrary but equal. Another simplification arises in Fourier space from translational invariance, because for two-time correlation functions (2.16) leads to the condition

$$\langle \delta f^*_{\boldsymbol{q}} e^{\Omega^\dagger t} \delta g_{\boldsymbol{q}'} \rangle^{(\dot{\gamma})} \stackrel{!}{=} e^{-i(\boldsymbol{q}'\cdot\kappa t + \boldsymbol{q}' - \boldsymbol{q})\cdot\boldsymbol{a}} \langle \delta f^*_{\boldsymbol{q}} e^{\Omega^\dagger t} \delta g_{\boldsymbol{q}'} \rangle^{(\dot{\gamma})} \,. \tag{2.20}$$

This equality holds for $e^{-i(\boldsymbol{q}'\cdot\kappa t + \boldsymbol{q}' - \boldsymbol{q})\cdot\boldsymbol{a}} = 1$, which only is the case for

$$\boldsymbol{q}' = \boldsymbol{q}(t) \equiv \boldsymbol{q} - \boldsymbol{q}\cdot\kappa t \tag{2.21}$$

with $\boldsymbol{q}(t)$ as the advected wavevector; all fluctuations with other wavevector combinations do not fulfil (2.20) [Fuc10].

This means that therefore all two-time correlations of fluctuations are decorrelated except for the one between the primary fluctuation and its shear-advected correspondent to a later time t. The concept of advected wavevectors takes account of this in an efficient way, subtracting trivial effects of flow from density correlators and focusses only on the non-trivial correlations. A detailed and colourful explanation of this concept can be found, e.g. in [Fuc10]. Figure 2.1 sketches the advection of a fluctuation in absence of Brownian motion.

Identifying $\boldsymbol{q}'$ in (2.20) with the advected wavevector makes it possible to define a stationary time-dependent correlation function also characterised by a single but

time-dependent wavevector [FC09]:

$$C_{fg;\boldsymbol{q}}(t,\dot{\gamma}) = \frac{1}{N}\langle \delta f^*_{\boldsymbol{q}} e^{\Omega^\dagger t}\delta g_{\boldsymbol{q}(t)}\rangle^{(\dot{\gamma})} \ . \tag{2.22}$$

For the further content of this elaboration the case of density fluctuations is of special interest, i.e. $f_{\boldsymbol{q}}(\Gamma,t) = g_{\boldsymbol{q}}(\Gamma,t) = \rho_{\boldsymbol{q}}(t)$. So the abbreviations $C_{\boldsymbol{q}}(t,\dot{\gamma}) = (1/N)\langle \delta\rho^*_{\boldsymbol{q}} e^{\Omega^\dagger t}\delta\rho_{\boldsymbol{q}(t)}\rangle^{(\dot{\gamma})}$ - denoting the intermediate scattering function - and $S_{\boldsymbol{q}}(\dot{\gamma}) = (1/N)\langle \delta\rho^*_{\boldsymbol{q}}\delta\rho_{\boldsymbol{q}}\rangle^{(\dot{\gamma})}$ for the equal-time structure factor shall be made. The former was found to be a real function and symmetric with respect to $\boldsymbol{q}$ [FC09]. Whenever the shear-dependence is not given explicitly, it shall be deemed to be the equilibrium quantity, i.e. $S_q \equiv (1/N)\langle \delta\rho^*_{\boldsymbol{q}}\delta\rho_{\boldsymbol{q}}\rangle$.

2.3. Integration Through Transients

In this chapter the Smoluchowski equation (2.5) will be solved in an exact formal way, approaching via the integration of the transient shear-dependent dynamics.

The starting position of the system - being in equilibrium for times $t \leq 0$ - with instantaneously applied shear at $t = 0$, which is held constant thereafter, can be implemented in the SO by the following way:

$$\Omega(\Gamma,t) = \begin{cases} \Omega_{\mathrm{e}}(\Gamma), & t \leq 0 \\ \Omega(\Gamma), & t > 0 \end{cases} \ . \tag{2.23}$$

Hence the formal solution for the time-dependent probability density is given by

$$\Psi(t) = e^{\Omega t}\Psi_{\mathrm{e}} \ . \tag{2.24}$$

The identity

$$e^{\Omega t} = 1 + \int_0^t \mathrm{d}t' e^{\Omega t'}\Omega \tag{2.25}$$

and the relation (2.11) can be used to obtain an expression for the unknown stationary distribution function $\Psi(t\to\infty) = \Psi_{\mathrm{s}}$:

$$\Psi_{\mathrm{s}} = \Psi_{\mathrm{e}} + \dot{\gamma}\int_0^\infty \mathrm{d}t\, \Psi_{\mathrm{e}}\sigma_{xy}e^{\Omega^\dagger t} \tag{2.26}$$

(remember $\Omega_{\mathrm{e}}\Psi_{\mathrm{e}} = 0$) [FC09]. It is composed by the equilibrium distribution and an integration of the transient dynamics containing slow intrinsic motion of the colloidal particles [Fuc10],[FC09]. As already mentioned at (2.12) the exponential functions act as time evolution operators for the distribution functions (and averaged quantities, respectively for the adjoint SO), driving these from start time t_0 to a later time t. The difference in using Ω or $\Omega^\dagger$ is similar to that of a Schrödinger

and a Heisenberg representation in quantum physics. As can be seen by calculating steady state averages with the solution in (2.26)

$$\langle f\rangle^{(\dot\gamma)} = \langle f\rangle + \dot\gamma \int_0^\infty \mathrm{d}t \langle \sigma_{xy} e^{\Omega^\dagger g} f\rangle \tag{2.27}$$

this is one of the key results of the MCT-ITT approach since it transforms stationary non-equilibrium averages of arbitrary quantities into equilibrium averages with the well known initial distribution function Ψ_e. Recalling the fact that steady state averages can be non-vanishing for zero wavevector only (2.18) a further simplification is possible [FC09], leading to

$$f(\dot\gamma) = \frac{\langle f_{\boldsymbol{q}=0}\rangle}{V} + \frac{\dot\gamma}{V}\int_0^\infty \mathrm{d}t \langle \sigma_{xy} e^{\Omega^\dagger t} \Delta f_{\boldsymbol{q}=0}\rangle \tag{2.28}$$

Here the relation $\langle \sigma_{xy} e^{\Omega^\dagger t} c\rangle = 0$ was used, which is valid for any constant c, because mean transverse stress vanishes in equilibrium. Thus, and also because all mean values in the ITT integral are constants, they are omitted in equation (2.28), leaving just the fluctuating parts $\Delta f_{\boldsymbol{q}=0}$ to appear in the integral [Fuc10; FC09]. Equation (2.28) represents a generalised Green-Kubo relation based on a transient correlation function. Applying it on the shear stress gives an exact non-linear Green-Kubo relation for the thermodynamic transverse stress, defining the generalised shear modulus $g(t,\dot\gamma)$:

$$\sigma_{xy}(\dot\gamma) \equiv \frac{\langle\sigma_{xy}\rangle^{(\dot\gamma)}}{V} = \dot\gamma \int_0^\infty \mathrm{d}t \underbrace{\frac{1}{V}\langle \sigma_{xy} e^{\Omega^\dagger t}\sigma_{xy}\rangle^{(\dot\gamma=0)}}_{\equiv g(t,\dot\gamma)} . \tag{2.29}$$

Before going to approximations, note that to ensure the convergence of the integral in (2.28) for long times, one has to avoid a zero eigenvalue of the adjoint SO, which may arise from the existence of conservation laws, e.g. the particle number of the considered system. This potentially causes a non-decaying contribution to the correlation function. With a projection method that is described in [For75] one can examine the distribution function coupling with the densities of the conserved quantities, i.e. number density $n = N/V$ in this case. In [FC05] density fluctuations were found not to couple linearly with the shear-distorted distribution function and therefore, number conservation does not cause a zero eigenvalue of $\Omega^\dagger$ [FC09].

This holds in the case of the exact dynamics, but when applying approximations the prevention of artificial couplings is indispensable. In linear order these can be avoided by a projection orthogonal to the one on density fluctuations, represented by the projectors Q and P, respectively:

$$Q = 1 - P, \qquad \text{with } P = \sum_{\boldsymbol{q}} \delta\rho_{\boldsymbol{q}} \rangle \frac{1}{NS_q} \langle \delta\rho^*_{\boldsymbol{q}} . \tag{2.30}$$

So the following identity is available

$$\langle \sigma_{xy} e^{\Omega^\dagger t} X \rangle = \langle \sigma_{xy} Q e^{\Omega^\dagger t} Q X \rangle = \langle \sigma_{xy} Q e^{Q\Omega^\dagger Q t} Q X \rangle \tag{2.31}$$

and can be used in turn to bring (2.28) into a form in which approximation much more safely can be performed [FC09]:

$$f(\dot{\gamma}) = \frac{\langle f_{\boldsymbol{q}=0} \rangle}{V} + \frac{\dot{\gamma}}{V} \int_0^\infty \mathrm{d}t \langle \sigma_{xy} Q e^{Q\Omega^\dagger Q t} Q \Delta f_{\boldsymbol{q}=0} \rangle \ . \tag{2.32}$$

Analogous formulas can be derived on identical lines including the previously introduced projection for the stationary time-dependent correlation functions from equation (2.22)

$$C_{fg;\boldsymbol{q}}(t, \dot{\gamma}) = \frac{\langle \delta f_{\boldsymbol{q}}^* e^{\Omega^\dagger t} \delta g_{\boldsymbol{q}(t)} \rangle}{N} + \frac{\dot{\gamma}}{N} \int_0^\infty \mathrm{d}t' \langle \sigma_{xy} Q e^{Q\Omega^\dagger Q t'} Q \Delta (\delta f_{\boldsymbol{q}}^* e^{\Omega^\dagger t} \delta g_{\boldsymbol{q}(t)}) \rangle \tag{2.33}$$

and for the structure functions defined in (2.19):

$$S_{fg;\boldsymbol{q}}(\dot{\gamma}) = \frac{\langle \delta f_{\boldsymbol{q}}^* \delta g_{\boldsymbol{q}} \rangle}{N} + \frac{\dot{\gamma}}{N} \int_0^\infty \mathrm{d}t' \langle \sigma_{xy} Q e^{Q\Omega^\dagger Q t} Q \Delta (\delta f_{\boldsymbol{q}}^* \delta g_{\boldsymbol{q}}) \rangle \ . \tag{2.34}$$

3. Mode Coupling Approximations

This chapter deals with the generalised Green-Kubo relations (2.32)-(2.34) that are developed in the last section, by applying approximations motivated by MCT. In this way the problem of calculating equilibrium averages shifts into one of integrating the transient response of the system after (steady) shear is switched on.

3.1. Coupling to Density Fluctuations

For further progress the following definition of the transient density correlator $\Phi_{\boldsymbol{q}}$ at wavevector $\boldsymbol{q}$ proofs crucial [Fuc10],[FC09]:

$$\Phi_{\boldsymbol{q}}(t) \equiv \frac{1}{NS_q}\langle \delta\rho^*_{\boldsymbol{q}} e^{\Omega^\dagger t}\delta\rho_{\boldsymbol{q}(t)}\rangle \ . \tag{3.1}$$

$\Phi_{\boldsymbol{q}}(t)$ is a correlation function of an equilibrium density fluctuation $\delta\rho^*_{\boldsymbol{q}}$ at initial time $t_0 = 0$ and the corresponding shear-advected fluctuation $\delta\rho_{\boldsymbol{q}(t)}$ at time $t > 0$, encoding the competition between random fluctuations and shear-driven motion. It also depends on the shear rate $\dot\gamma$, which is notationally suppressed and is a real and symmetric quantity: $\Phi^*_{\boldsymbol{q}}(t) = \Phi_{\boldsymbol{q}}(t) = \Phi_{-\boldsymbol{q}}(t)$. Without particle interactions and Brownian motions holds $\Phi_{\boldsymbol{q}}(t) \equiv 1$ [Fuc10]. This important quantity is discussed in detail in section 4.2. Although the transient correlator and the stationary intermediate scattering function $C_{\boldsymbol{q}}(t,\dot\gamma)$ are of similar shape, there is an important conceptual difference. While the first matches the initial (equilibrium) state and a non-equilibrium state at finite time t after startup of shear, the latter describes correlations between two non-equilibrium but stationary states long after startup, separated by a time t. However, in the following approximation scheme these two were found in [FC09] to differ only by a static renormalisation of the amplitude and to coincide at time zero.

The expressions (2.32)-(2.34) can essentially be traced back to correlations in the form of $\langle \sigma_{xy} Q e^{Q\Omega^\dagger Q t} Q\Delta X\rangle$, where ΔX denotes a general fluctuation. This correlator represents the stochastic overlap of a stress fluctuation appeared at time zero with the general fluctuation ΔX that was driven until time t by shear and internal motion. Now its magnitudes shall be approximated following the way developed in [FC09] (including results from [Kaw70]) by using static overlaps of density fluctuation pairs with the fluctuations of both ΔX and stress; because those describe

the relevant structural rearrangements. These overlaps can be implemented via projectors in the form of

$$\sum_{\boldsymbol{k}>\boldsymbol{p}} \delta\rho_{\boldsymbol{k}}\delta\rho_{\boldsymbol{p}} \rangle \frac{1}{N^2 S_k S_p} \langle\ \delta\rho^*_{\boldsymbol{k}}\delta\rho^*_{\boldsymbol{p}} \tag{3.2}$$

using the Gaussian approximation $\langle\delta\rho^*_{\boldsymbol{k}}\delta\rho^*_{\boldsymbol{p}}\delta\rho_{\boldsymbol{k}'}\delta\rho_{\boldsymbol{p}'}\rangle \approx N^2 S_k S_p \delta_{\boldsymbol{k},\boldsymbol{k}'}\delta_{\boldsymbol{p},\boldsymbol{p}'}$ and the order $k > p$, $k' > p'$.

This step can on the one hand be done for time-dependent transient correlators of arbitrary functions of particle positions that do not couple with density in linear order [FC09]:

$$\begin{aligned}&\langle\delta f^*_{\boldsymbol{q}(-t)} Q e^{Q\Omega^\dagger Q t} Q\delta g_{\boldsymbol{q}}\rangle \approx \\ &\sum_{\boldsymbol{k}>\boldsymbol{p}}\sum_{\boldsymbol{k}'>\boldsymbol{p}'} \frac{\langle\delta f^*_{\boldsymbol{q}(-t)} Q\delta\rho_{\boldsymbol{k}'}\delta\rho_{\boldsymbol{p}'}\rangle}{N^2 S_{k'} S_{p'}} \langle\delta\rho^*_{\boldsymbol{k}'}\delta\rho^*_{\boldsymbol{p}'} e^{Q\Omega^\dagger Q t}\delta\rho_{\boldsymbol{k}}\delta\rho_{\boldsymbol{p}}\rangle \frac{\langle\delta\rho^*_{\boldsymbol{k}}\delta\rho^*_{\boldsymbol{p}} Q\delta\rho_{\boldsymbol{q}}\rangle}{N^2 S_k S_p}\ .\end{aligned} \tag{3.3}$$

By replacing the four-density average by a product of pair averages and using the full dynamics instead of the reduced dynamics - which is comparable to a shift from the reduced SO $Q\Omega^\dagger Q$ to the full one $\Omega^\dagger$ - one arrives at

$$Q e^{Q\Omega^\dagger Q t} Q \approx \sum_{\boldsymbol{k}>\boldsymbol{p}} Q\delta\rho_{\boldsymbol{k}(-t)}\delta\rho_{\boldsymbol{p}(-t)} \rangle \frac{\Phi_{\boldsymbol{k}(-t)}(t)\Phi_{\boldsymbol{p}(-t)}(t)}{N^2 S_k S_p} \langle\ \delta\rho^*_{\boldsymbol{k}}\delta\rho^*_{\boldsymbol{p}} Q\ . \tag{3.4}$$

This defines a rule valid for all those fluctuation products (of non-coupling variables) which holds for slow structural relaxations [FC09]. It is visible, that the step of inserting the full dynamics is equivalent to approximating the time evolution by the transient density correlator.

On the other hand this can also be done for fluctuations that are able to couple in linear order with densities (in a way similar to the one just discussed [FC09]) to derive a second rule

$$e^{\Omega^\dagger t} \approx \sum_{\boldsymbol{q}} \delta\rho_{\boldsymbol{q}(-t)} \rangle \frac{\Psi_{\boldsymbol{q}(-t)}(t)}{N S_q} \langle\ \delta\rho^*_{\boldsymbol{q}}\ . \tag{3.5}$$

To summarize the main steps: In both cases the fluctuating variables are projected onto density fluctuations and pairs of them respectively, while the reduced dynamics were replaced by the full dynamics. Note that all averages are of equilibrium type, which can due to the ITT formalism be used to calculate stationary states far from equilibrium as detailed in the next section.

3.2. Approximated Green-Kubo Relations

The projection step introduced in the last section can now be applied on exact Green-Kubo relations (2.32)-(2.34) to obtain approximated expressions of stationary averages, time-dependent correlation functions and the structure functions from (2.19).

3.2.1. General Stationary Expectation Values

The first approximation rule developed in the last section can now be implemented in the exact expression for arbitrary steady state averages (2.32). This leads to

$$f(\dot{\gamma}) \approx \frac{\langle f_0 \rangle}{V} + \frac{\dot{\gamma}}{2V} \int_0^\infty \mathrm{d}t \sum_{\boldsymbol{k}} \frac{k_x k_y(-t) S'_{k(-t)}}{k(-t) S_k^2} V_{\boldsymbol{k}}^f \Phi^2_{\boldsymbol{k}(-t)}(t) \; . \tag{3.6}$$

The derivative with respect to a wavevector is thereby notated as $S'_k \equiv \partial S_k / \partial k$ [FC09]. The coupling of f with density pairs is described by the vertex $V_{\boldsymbol{k}}^f$:

$$V_{\boldsymbol{k}}^f \equiv \frac{\langle \delta\rho^*_{\boldsymbol{k}} \delta\rho_{\boldsymbol{k}} Q \Delta f_0 \rangle}{N} = \frac{\langle \delta\rho^*_{\boldsymbol{k}} \delta\rho_{\boldsymbol{k}} \Delta f_0 \rangle}{N} - S_0 \left(S_k + n \frac{\partial S_k}{\partial n} \right) \left(\frac{\partial f^{\mathrm{eq}}}{\partial n} \right)_T \; . \tag{3.7}$$

Here some thermodynamic relations were used in order to derive the second term [FC09]. One refers to the thermodynamic derivative $(\partial f^{\mathrm{eq}}/\partial n)_T$, which appears to be the zero-wavevector limit of $\langle \rho^*_{\boldsymbol{q}} \Delta f q \rangle / \langle |\delta\rho_{\boldsymbol{q}}|^2 \rangle$ found by [For75] - where $f^{\mathrm{eq}} \equiv \langle f_0 \rangle / V$. The other is the relation by [Bax64] giving $\langle \delta\rho^*_{\boldsymbol{q}} \delta\rho_{\boldsymbol{k}} \delta\rho_0 \rangle = N S_0 \left[S_k + n \left(\partial S_k / \partial n \right) \right]$ that must though handled carefully, since it influences the limiting behaviour of the structural distortion in (3.15) [FC09].

Using the general formula (3.7) the stationary expectation value of the shear stress of a homogeneously sheared dispersion can be computed [FC09], which is discussed in detail in section 6.1:

$$\sigma_{xy}(\dot{\gamma}) \approx \frac{\dot{\gamma}}{2} \int_0^\infty \mathrm{d}t \underbrace{\int \frac{\mathrm{d}^3 k}{(2\pi)^3} \frac{k_x^2 k_y k_y(-t)}{k k(-t)} \frac{S'_k S'_{k(-t)}}{S_k^2} \Psi^2_{\boldsymbol{k}(-t)}(t)}_{\approx 2g(t,\dot{\gamma})} \tag{3.8}$$

(where $\langle \sigma_{xy} \rangle = 0$ was used again).

3.2.2. Time-Dependent Correlation Functions

For the sake of completeness an expression for the intermediate scattering function as an occurrence of the time-depending correlation function (2.33) will also be given here in this approximation. The derivation continues along an analogous way as in the last subsection to obtain (3.8) - with the distinction that the evolution operator $e^{\Omega^\dagger}$ may couple linearly to density in $C_{fg;\boldsymbol{q}}(t, \dot{\gamma})$. Hence, beside the first approximation rule (3.4) the second rule also has to be applied on the t-dependence [FC09], leading to

$$C_{\boldsymbol{q}}(t, \dot{\gamma}) = \left[S_q + \frac{\dot{\gamma}}{N} \int_0^\infty \mathrm{d}t' \langle \sigma_{xy} Q e^{Q\Omega^\dagger Q t'} Q \Delta(\delta\rho^*_{\boldsymbol{q}} \delta\rho_{\boldsymbol{q}}) \rangle \right] \Phi_{\boldsymbol{q}}(t) \; . \tag{3.9}$$

Detailed discussion of this quantity can be found, e.g. in [Zau+08] - in particular about the differences between the transient and stationary correlators pointed out before - or in [KGF09] - which discusses an extension of this approximation scheme - and are not content of this elaboration.

3.2.3. Distorted Structure Functions

Applying the approximation (3.4) to the structure functions (2.34) leads to the general result

$$S_{fg;\boldsymbol{q}}(\dot{\gamma}) \approx \frac{\langle \delta f^*_{\boldsymbol{q}} \delta g_{\boldsymbol{q}} \rangle}{N} + \frac{\dot{\gamma}}{2N} \int_0^\infty \mathrm{d}t \sum_{\boldsymbol{k}} \frac{k_x k_y(-t) S'_{k(-t)}}{k(-t) S_k^2} V_{\boldsymbol{k}}^{fg} \Phi^2_{\boldsymbol{k}(-t)}(t) \tag{3.10}$$

with the vertex function defined similarly to (3.7):

$$V_{\boldsymbol{k}}^{fg} \equiv \frac{\langle \delta\rho^*_{\boldsymbol{k}} \delta\rho_{\boldsymbol{k}} Q \Delta (\delta f^*_{\boldsymbol{q}} \delta g_{\boldsymbol{q}}) \rangle}{N} \tag{3.11}$$

as done in [FC09]. For the special case of density fluctuations, the concrete representation can be obtained by using again the relation in [Bax64], that was also taken into account to derive (3.7):

$$V_{\boldsymbol{k}}^{\rho^*_{\boldsymbol{q}}\rho_{\boldsymbol{q}}} \equiv \frac{\langle \delta\rho^*_{\boldsymbol{k}} \delta\rho_{\boldsymbol{k}} Q \Delta (\delta\rho^*_{\boldsymbol{q}} \delta\rho_{\boldsymbol{q}}) \rangle}{N} = 2N S_q^2 \delta_{\boldsymbol{qk}} - S_0 \left(S_k + n \frac{\partial S_k}{\partial n} \right) \frac{\partial}{\partial n} (n S_q) \,. \tag{3.12}$$

From this vertex the MCT-ITT expression for the distorted structure factor under shear arises as follows [FC09]:

$$S_{\boldsymbol{q}}(\dot{\gamma}) \approx S_q + \delta S^{\mathrm{aniso}}_{\boldsymbol{q}}(\dot{\gamma}) + \delta S^{\mathrm{iso}}_q(\dot{\gamma}) \tag{3.13}$$

with an anisotropic and an isotropic contribution distorting the equilibrium structure factor

$$\delta S^{\mathrm{aniso}}_{\boldsymbol{q}} = \dot{\gamma} \int_0^\infty \mathrm{d}t \frac{q_x q_y(-t)}{q(-t)} S'_{q(-t)} \Phi^2_{\boldsymbol{q}(-t)}(t) \,, \tag{3.14}$$

$$\begin{aligned} \delta S^{\mathrm{iso}}_q = {} & \frac{\dot{\gamma} S_0}{2n} \left(S_q + n \frac{\partial S_q}{\partial n} \right) \\ & \times \left\{ \int_0^\infty \mathrm{d}t \int \frac{\mathrm{d}^3 k}{(2\pi)^3} \frac{k_x k_y(-t)}{k(-t) S_k^2} S'_{k(-t)} \left(S_k + n \frac{\partial S_k}{\partial n} \right) \Phi^2_{\boldsymbol{k}(-t)}(t) \right\} \,. \end{aligned} \tag{3.15}$$

Unfortunately the isotropic part remains finite for large wavevectors because of the relation in [Bax64], so the distorted structure does not fulfil $S_{\boldsymbol{q}\to\infty}(\dot{\gamma}) \to 1$ as required, since all intermolecular contributions have to disappear in the large-wavevector limit. This may be a hint for the scope of the approximations, as they appear unable to reproduce the very local correlations. Perhaps the reason can be found to be located in the calculation of Baxter's relation as suggested above [FC09].

The numerical calculation of distorted structure and its effects on stress and local pair order are the major subjects in this elaboration. Equation (3.13) is discussed in detail in chapter 5, whereas its consequences are content of chapters 6 and 7.

3.3. Transient Structural Relaxations

Since the approximations above merely depend on the transient dynamics and the equilibrium structure, the remaining step to complete the presented theory and receive a closed set of equations is to give expressions from which the transient density correlator from (3.1) can be determined. Its equation of motion is in the same framework developed in [FC09], giving

$$\partial_t \Phi_{\boldsymbol{q}}(t) + \Gamma_{\boldsymbol{q}}(t) \left\{ \Phi_{\boldsymbol{q}}(t) + \int_0^t \mathrm{d}t' \, \overline{m}_{\boldsymbol{q}(-t')}(t-t') \, \partial_{t'} \Phi_{\boldsymbol{q}}(t') \right\} = 0 \tag{3.16}$$

where the initial decay rate is given by $\Gamma_{\boldsymbol{q}} = q^2(t)/S_{q(t)}$. The approximated memory function $\overline{m}_{\boldsymbol{q}}$ and its vertices

$$\overline{m}_{\boldsymbol{q}'}(\tau) = \frac{1}{2N} \sum_{\boldsymbol{k}'} \frac{S_{q'(\tau)} S_{k'} S_{p'}}{q'^2(\tau) q'^2} V_{\boldsymbol{q}'\boldsymbol{k}'\boldsymbol{p}'}(\tau) V_{\boldsymbol{q}'\boldsymbol{k}'\boldsymbol{p}'}(\tau) \, \Phi_{\boldsymbol{k}'}(\tau) \Phi_{\boldsymbol{p}'}(\tau) \tag{3.17}$$

$$V_{\boldsymbol{q}\boldsymbol{k}\boldsymbol{p}} = \frac{\langle \rho^*_{\boldsymbol{q}} \Omega^\dagger_{\mathrm{e}} Q \rho_{\boldsymbol{k}} \rho_{\boldsymbol{p}} \rangle}{N S_k S_p} = \boldsymbol{p} \cdot (\boldsymbol{k} n c_k + \boldsymbol{p} n c_p) \delta_{\boldsymbol{q}, \boldsymbol{k}+\boldsymbol{p}} \tag{3.18}$$

capture the autocorrelations of fluctuating stresses involving density correlators [FC09]. Here the abbreviations $\boldsymbol{p}' = \boldsymbol{q}' - \boldsymbol{k}'$ and $c_k = (1 - 1/S_k)/n$ for the Ornstein-Zernicke direct correlation function were made.

With these equations the transient density correlator can be found and therefore used to calculate the generalised Green-Kubo relations (2.32)-(2.34) with the system's equilibrium structure factor as the only input. Numerical solutions of (3.16) can be found, e.g. in [Hen+09] and [KWF11] and will be used in the following chapters.

4. Equilibrium and Transient Quantities

In the developed mode coupling approach (followed the lines of [Fuc10; FC09]) exact relations for stationary averages, correlators and structure functions are related to equilibrium averages of the transient dynamics with the initial distribution. By approximations motivated from MCT the problem of calculating averages was shifted to integrating the slow structural rearrangements after startup of the shear encoded in the transient density correlator - defined in (3.1) and determined by its equation of motion.

On this background the effect of shear on the microscopic structure seemed interesting to calculate including the isotropic contributions, which were neglected in former investigations, e.g. [Zau+08; FC09; Hen+09; Ama+15]. Because the properties of the stationary shear-distorted quantities from the approximated Green-Kubo relations are mainly dependent on the transient response of the system, the equilibrium structure factor and the transient correlators are discussed in this chapter.

4.1. Equilibrium Structure Factor

The microscopic structure in thermal equilibrium S_q appears to be the only input in the MCT-ITT formalism. It is the Fourier transform of the pair correlation function and gives information about the microscopic order of the system. S_q is defined as a correlation function of density Fourier components (as done at the end of section 2.2).

Figure 4.1 shows the two-dimensional structure factors S_q of monodisperse hard discs for different packing fractions $\eta = n\pi/4$, which is the only thermodynamic control parameter of the system. The data were obtained with a modified hypernetted chain closure [Kb] and used in further calculations (see chapters 5 and 6).

In contrast to an ideal gas, where the local density is equal to its average and therefore the positions of adjacent particles are nearly uncorrelated, a liquid exhibits a short range order indicated by the large first peak in S_q and rapidly damped oscillations. In the limit of large wavevectors only the self-correlations survive leading to $S_{q\to\infty} = 1$. The primary peak occurring at $q_\mathrm{p}d \approx 6.6 \approx 2\pi$ reflects a shell of neighbouring particles close to the contact value $r/d = 1$.

As can be seen in figure 4.1 S_q depends smoothly on the packing fraction η.

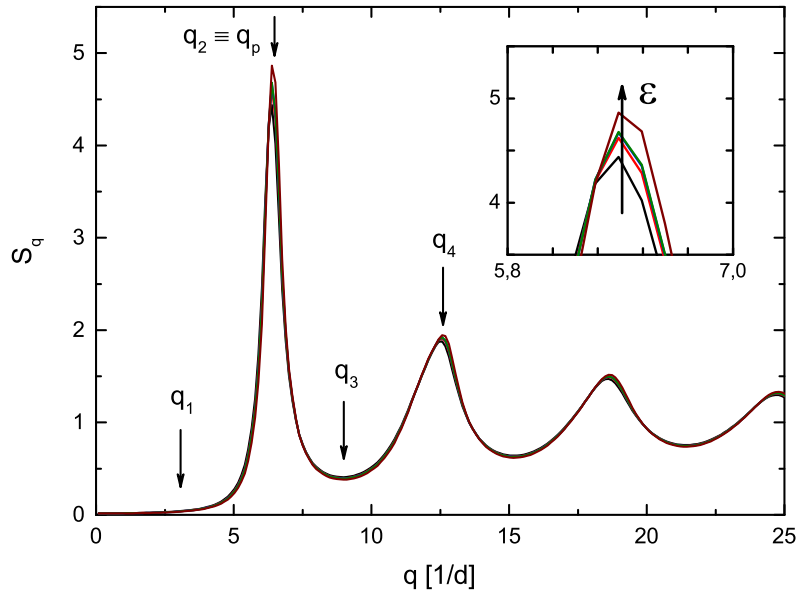

Figure 4.1.: Equilibrium structure factor S_q from [Kb] obtained by a modified hypernetted chain closure, for separation parameters $\epsilon = -10^{-2}$ (black), $-1.6 \cdot 10^{-3}$ (red), $6.3 \cdot 10^{-4}$ (blue), 10^{-3} (green) and 10^{-2} (brown); the distinguished wavevectors are $q_1 \approx 3$, $q_\mathrm{p} \approx 6.6$, $q_3 \approx 9$ and $q_4 \approx 12.6$. The inset shows the primary peak, increasing with densification.

However, at a critical packing η_c it causes a phase transition from a fluid to a glassy state which appears to yield due to applied shear. To measure the distance to the transition it is convenient to introduce the separation parameter $\epsilon \equiv (\eta - \eta_c)/\eta_c$, corresponding to a fluid regime for negative values ($\epsilon < 0$) and a glassy state for $\epsilon > 0$. Densification induces a pronounced order within a few particle diameters which is reflected by increasing peaks - especial at $q = q_p$ [Hen+09]. Since without shear the dynamic of the system does not distinguish a certain direction, the equilibrium structure factor depends on the wavevector-magnitude only and is thus isotropic.

While MCT calculations are possible for a monodisperse system only (since bidisperse systems are to costly in time and memory [Hen+09]), experiments and MD simulations typically deal with dispersions containing colloids of two different diameters in order to avoid crystallisation. Averaged structure factors of such bidesperse systems are shown, e.g. in [Hen+09]. They have major qualitative differences beyond the second peak of S_q, hence comparisons can carefully be made for small wavevectors only. A detailed discussion of equilibrium structure factors, their connection to the pair structure in real space and the experimental relevance can be found, e.g. in [BH03] or [HM06].

4.2. Transient Density Correlator

As detailed at the definition (3.1) the transient density correlation functions contain the transient structural rearrangements caused by shear. Figure 4.2 shows the correlators $\Phi_{\boldsymbol{q}}(t)$ for different separation parameters ϵ and different shear rates $\dot{\gamma}$. Its qualitative behaviour is basically ruled by two mechanisms, apparent by two individual decays, which are the content of this section.

Brownian Motion

The random movement of the particles causes a decorrelation of thermal fluctuations reflected by a first decay of $\Phi_{\boldsymbol{q}}(t)$, which can be seen in figure 4.2. The expansion $\Phi_{\boldsymbol{q}}(t \to 0) \to 1 - \Gamma_{\boldsymbol{q}}(0)t + \dots$ shows that the short time behaviour is dominated by the initial decay rate containing the diffusion coefficient of a single particle D_0. Thus, in absence of Brownian motion (viz. $D_0 = 0$) the correlator will not decay at all; even not for finite shear rates, since the advected wavevectors perfectly keep track of the shear-induced affine particle motion (cf. figure 2.1) [FC09],[Fuc10].

Remembering the definition of $\Gamma_{\boldsymbol{q}}(t)$ in section 3.3 shows that the initial decay rate is smallest at the first peak of S_q causing the correlator to decay most slowly at q_p (cf. figure 4.2); this means that structural fluctuations survive longest on small spatial distances around the contact value. In figure 4.2 also is visible that in the quiescent fluid state ($\epsilon < 0$) Brownian motion causes $\Phi_q^{\dot{\gamma}=0}$ to decay completely for long times; on the contrary it reaches a plateau level for $\epsilon > 0$ which marks, that the systems is arrested in a metastable glassy state. Since Brownian motion does not emphasise a special direction, the first decay is isotropic [KWF11; Hen+09].

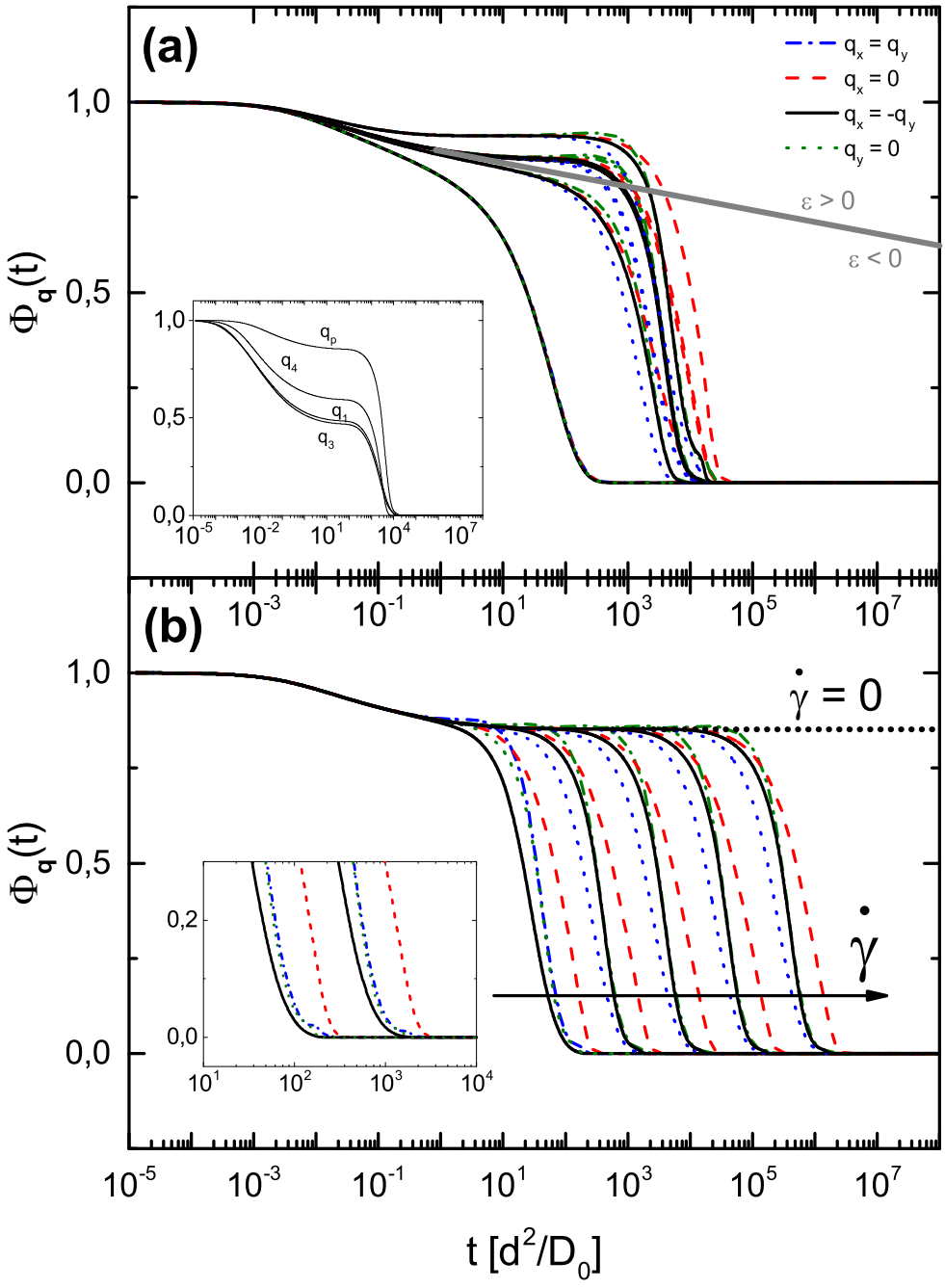

Figure 4.2.: Radial cuts through the transient density correlators $\Phi_{\boldsymbol{q}}(t)$ from [KWF11] as functions of time t; directions as indicated. **(a)** $\Phi_{\boldsymbol{q}}(t)$ for $\dot\gamma = 10^{-4}$ and different separation parameters $\epsilon = -10^{-2}, -1.6{\cdot}10^{-3}, 6.3{\cdot}10^{-4}, 10^{-3}$ and 10^{-2} (from the bottom up) at wavevector q_p; the inset shows density correlators with $\epsilon = 10^{-3}$, $\dot\gamma = 10^{-4}$ for the different wavevectors $q_1 \approx 3$, $q_\mathrm{p} \approx 6.6$, $q_3 \approx 9$ and $q_4 \approx 12.6$. **(b)** $\Phi_{\boldsymbol{q}}(t)$ for $\epsilon = 10^{-3}$ and different Péclet numbers $\mathrm{Pe}_0 = 10^{-m}$ with $m \in \{2, 3, 4, 5, 6\}$ (from left to right) at wavevector q_p; the inset resolves the anisotropy at the end of the alpha relaxation for $\mathrm{Pe}_0 = 10^{-2}$ and 10^{-3}.

Shear-Induced Flow
The origin of the second decay is the so called α-relaxation caused by shear, forcing the system to yield - because of shear-melting in the glassy case. For strongly viscoelastic systems as the present one, this effect is already measurable for very small shear rates $1 \gg \dot{\gamma}$ [Hen+09; Bay+07]. An established quantity for the competition between shear and Brownian dynamics is the bare Péclet number Pe_0. It measures the affine particle motion with the sheared solvent relative to the time a single Brownian particle needs to diffuse its own diameter. In the chosen unit convention Pe_0 is equal to the shear rate $\dot{\gamma}$ [FC09]. The α-decay depends on the flow profile and is therefore in principle anisotropic, i.e. in the flow direction (x-direction in this case) the fluctuations are faster decorrelated as in the direction perpendicular to the flow. The diagonal $q_x = -q_y$ shows the quickest decay and is called compressional axis, followed by $q_x = q_y$ - the extensional axis (the origin of this nomenclature is discussed in detail in section 5.1.1). Close to the glass transition this anisotropy is quite small and merely can be found at $q \approx q_\mathrm{p}$ but grows deeper in the glass and depends strongly on the shear rate [Hen+09; Bay+07; KWF11]. Although it is notationally suppressed, yet apparent in figure 4.2, close to the glass transition $\Phi_{\boldsymbol{q}}(t)$ depends highly sensitive on the packing fraction η, so that the relaxation time increases strongly with densification and diverges in the glassy state.

The MCT-ITT formalism found the transient correlators approaching a master function for $\epsilon \geq 0$ and $\dot{\gamma} \to 0$; this only depends on the accumulated strain $\gamma = \dot{\gamma}t$ that appears as rescaled time. The theoretical background of this behaviour and numerical approaches are discussed in detail in [Fuc10] and [Hen+09; KWF11] (also for the incoherent case), respectively. In [KWF11] equation (3.16) was solved numerically using the equilibrium structure factor from [Kb] which is described in section 4.1. In contrast to [Hen+09] they chose a spherical grid, which will be introduced in section 4.3, while the latter used a Cartesian discretisation. The results from [KWF11] are shown in figure 4.2 used as input in this elaboration to calculate the ITT formulas (3.13) and (6.2) for the structural distortion and the stress.

4.3. Numerical Aspects

The numerical calculation of the distorted microstructure under shear was performed in two dimensions for hard discs of equal diameter d. A spherical discretisation of the Fourier space was chosen in order to properly resolve the anisotropy, since for constant q (in principle) all angles φ are available. The radial axis was divided in 100 points, starting with $q_0 d = 0.2$ and a separation $\Delta q d = 0.4$ which results in a cutoff of $qd = 39.8$. In angular direction the grid consists of 96 points from $\varphi_0 \approx \pi/48$ divided by $\Delta\varphi \approx \pi/48$; this means more explicitly $q \in \{0.2, 0.6, 1, \ldots, 39.8\}$ and $\varphi \in \{0.065, 0.131, 0.196, \ldots, 6.283\}$. Concerning the number of points in the angular space it is possible to make the radial cuts in the four characteristic directions $q_x = q_y$, $q_x = 0$, $q_x = -q_y$ and $q_y = 0$ - corresponding

to $\varphi = \pi/4$, $\varphi = \pi/2$, $\varphi = 3\pi/4$ and $\varphi = \pi$.

Time integrals were computed with an initial step of $1.28 \cdot 10^{-5} d^2/D_0$ switching to a step size of $2 \cdot 10^{-7} d^2/D_0$. After each 63 steps the step size was doubled resulting in a quasi-logarithmic grid in time.

This discretisation is the same which was used in [KWF11] to calculate the transient density correlators and leads to a critical packing fraction $\eta_c = 0.6985658$ [KWF11]. This differs slightly from that one which was obtained with a Cartesian discretisation in [Hen+09]. More numerical details are given in the appendix A.

5. Distorted Structure

In this chapter the results for the MCT-ITT approximation (3.13) of the distorted micro-structure under shear are calculated using the equilibrium structure and the transient density correlators from [Kb] and [KWF11] respectively, which are the topic of the last section. The results are presented and discussed pertaining to their stationary properties and their transient behaviour.

5.1. Steady State Properties

5.1.1. Anisotropic Distortion

In two dimensions and by using polar coordinates $\boldsymbol{q} \equiv q\,(\cos\vartheta, \sin\vartheta)^{\mathrm{T}}$ the anisotropic distorting contribution to the stationary structure factor $S_{\boldsymbol{q}}(\dot\gamma)$ from equation (3.14) becomes

$$\delta S_{\boldsymbol{q}}^{\mathrm{aniso}}(\dot\gamma) = \dot\gamma \int_0^\infty \mathrm{d}t \frac{q}{q(-t)} \left(\frac{1}{2} \sin 2\varphi + \dot\gamma t \cos^2\varphi \right) S'_{q(-t)} \Phi^2_{\boldsymbol{q}(-t)}(t) \tag{5.1}$$

where the magnitude of an advected wavevector is given by

$$q(-t) = q\sqrt{1 + \dot\gamma t \sin 2\varphi + (\dot\gamma t \cos\varphi)^2}\,. \tag{5.2}$$

The Substitution $\frac{\mathrm{d}}{\mathrm{d}t} S_{q(-t)} = \dot\gamma \frac{q}{q(-t)} \left(\frac{1}{2} \sin 2\varphi + \dot\gamma t \cos^2\varphi \right) S'_{q(-t)}$ (from [FC09]) leads to

$$\delta S_{\boldsymbol{q}}^{\mathrm{aniso}}(\dot\gamma) = \dot\gamma \int_0^\infty \mathrm{d}t \left(\frac{\mathrm{d}}{\mathrm{d}t} S_{q(-t)} \Phi^2_{\boldsymbol{q}(-t)}(t) \right) \tag{5.3}$$

which points out, that the anisotropic distortion is caused by the interplay of the structural rearrangements and the shear-induced stretching of density fluctuations. By replacing $\Phi_{\boldsymbol{q}}(t)$ with its master function and integrating over the rescaled time γ a yield value of the structural distortion was found in [FC09] causing a dynamic yield contribution to the structure factor that is explicitly independent of the shear rate.

The integration was performed for different shear rates corresponding to the Péclet numbers $\mathrm{Pe}_0 = 10^{-m}$ with $m \in \{2, 3, 4, 5, 6\}$ and, for $m = 4$, for different separation parameters $\epsilon \in \{-10^{-2}, -1.6 \cdot 10^{-3}, 6.3 \cdot 10^{-4}, 10^{-3}, 10^{-2}\}$. Figures 5.1 and 5.2 show radial cuts through the anisotropic contribution to the distorted structure in the four characteristic directions ($q_x = q_y$, $q_x = 0$, $q_x = -q_y$ and $q_y = 0$).

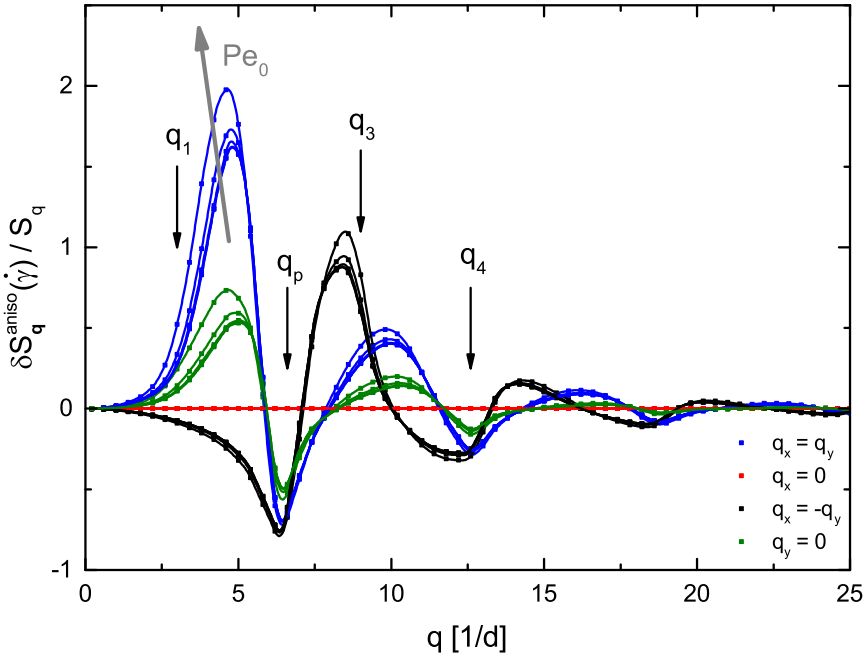

Figure 5.1.: Radial cuts through the normalised anisotropic structural distortion $\delta S_{\boldsymbol{q}}^{\text{aniso}}(\dot{\gamma})/S_q$ for the four characteristic directions as indicated; different shear rates, corresponding to Péclet numbers $\text{Pe}_0 = 10^{-m}$ with $m \in \{2,3,4,5,6\}$ (from bottom up) for a separation parameter $\epsilon = 10^{-3}$; the distinguished wavevectors are $q_1 \approx 3$, $q_\text{p} \approx 6.6$, $q_3 \approx 9$ and $q_4 \approx 12.6$.

As can be seen by (5.1) the distortion is shaped by the angular dependence of the trigonometric functions, which enlarge contributions in directions diagonal to the flow, whereas the perpendicular direction is totally suppressed; the flow direction dominates for $\dot{\gamma}t > 1$. The oscillations on the radial axis decay rapidly for larger q.

In the shear-melted glassy state for $\epsilon = 10^{-3}$ (see figure 5.1) the largest amplitudes of the distortion appear at small wavevectors around the main peak of S_q. In the area around q_p $\delta S_{\boldsymbol{q}}^{\text{aniso}}(\dot{\gamma})$ is negative and reaches a minimum in all directions which decreases the primary peak of the equilibrium S_q; the zeros in this area indicate instead that the peak is displaced.

In the direction $q_x = -q_y$ the distortion is positive for $q \gtrsim q_\text{p}$ which enhances the slope of the main peak in $S_{\boldsymbol{q}}(\dot{\gamma})$ at larger wavevectors. For $q \lesssim q_\text{p}$ it reaches a negative minimum, suppressing the low-q wing. Thus, the primary peak in the distorted structure is displaced to larger wavevectors along $q_x = -q_y$ reflecting the shear-flow induced compression of particles along this *compressional axis*. In contrast the direction $q_x = q_y$ shows a roughly inverse behaviour; there $\delta S_{\boldsymbol{q}}^{\text{aniso}}(\dot{\gamma})$

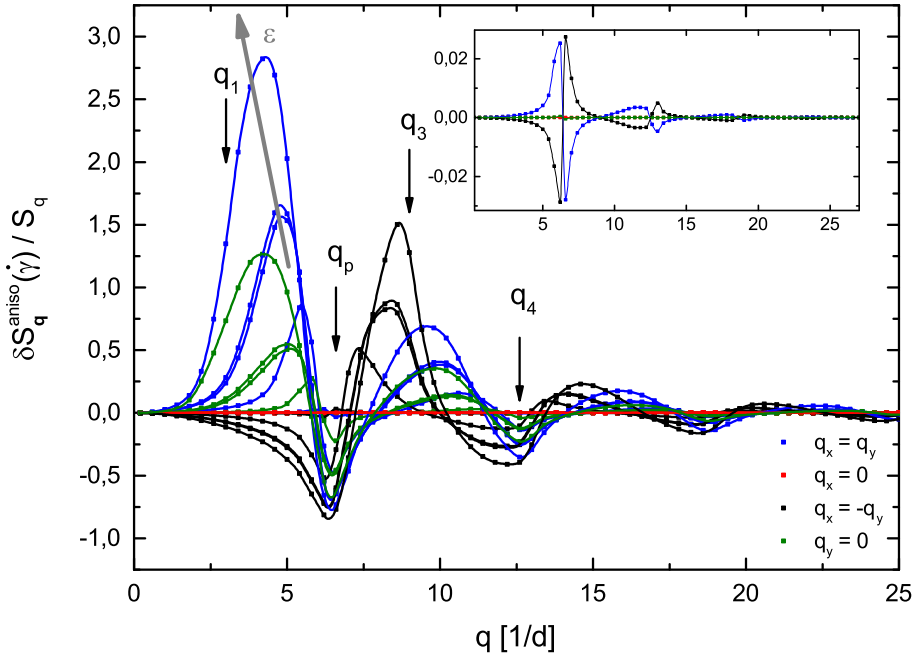

Figure 5.2.: Radial cuts through the normalised anisotropic structural distortion $\delta S_{\boldsymbol{q}}^{\mathrm{aniso}}(\dot{\gamma})/S_q$ for the four characteristic directions as indicated and for different separation parameter $\epsilon = -10^{-2}$, $-1.6 \cdot 10^{-3}$, $6.3 \cdot 10^{-4}$, 10^{-3} and 10^{-2} (from bottom up) for a Péclet number $\mathrm{Pe}_0 = 10^{-4}$. The lower inset shows $\delta S_{\boldsymbol{q}}^{\mathrm{aniso}}(\dot{\gamma})/S_q$ for the two fluid states ($\epsilon < 0$).

reaches its maximum at $qd \approx 4.7$ and has its global minimum close to q_{p}, shifting the primary peak to smaller wavevectors. This defines an *extensional axis* where the neighbouring particles are moved apart by shear. The direction $q_y = 0$ behaves quite similar to the extensional diagonal but with smaller amplitudes and its counterpart $q_x = 0$ is zero, since it is totally suppressed by the trigonometric functions.

This leads to an elliptical shape of the distorted microstructure for small wavevectors around q_{p}, which is visible in figure 5.1. The anisotropy of $\delta S_{\boldsymbol{q}}^{\mathrm{aniso}}(\dot{\gamma})$ decreases rapidly for larger wavevectors, so that $S_{\boldsymbol{q}}(\dot{\gamma})$ remains almost isotropic already beyond its second peak ($q > q_4$). Higher shear rates increase the magnitude of the anisotropic distortion, whereas its roots are not affected by different Pe_0. Hence the elliptical shape of $\delta S_{\boldsymbol{q}}^{\mathrm{aniso}}(\dot{\gamma})$ is somewhat elongated along the compressional diagonal for larger Péclet numbers compared to smaller Pe_0.

Variation of the packing fraction for small Pe_0 does strongly affect the distorted structure, as visible in figure 5.2. The amplitude of $\delta S_{\boldsymbol{q}}^{\mathrm{aniso}}(\dot{\gamma})$ decreases for smaller ϵ. In particular the first maximum shrinks highly - however, the first minimum does not - which leads finally to rather symmetric first peaks around the zero-axis

in the fluid state for $\epsilon = -10^{-2}$ (see the inset in figure 5.2). In this regime the anisotropic distortion is very small and therefore $S_{\boldsymbol{q}}(\dot\gamma)$ is almost isotropic.

5.1.2. Isotropic Distortion

By transforming equation (3.15) as detailed in section A.2 the isotropic contribution to the shear-distorted structure takes the following form

$$\delta S_q^{\mathrm{iso}}(\dot\gamma) = -\dot\gamma \frac{S_0}{2n}\left(S_q + n\frac{\partial S_q}{\partial n}\right)\,\mathcal{I}(t=\infty) \tag{5.4}$$

with the integral

$$\mathcal{I}(t) = \frac{1}{4\pi^2}\int_0^t \mathrm{d}t' \int_0^\infty \mathrm{d}k' \int_0^{2\pi} \mathrm{d}\varphi' k'^2 \frac{\sin 2\varphi'}{2}\frac{S'_{k'}}{S_k^2}\left(S_k + n\frac{\partial S_k}{\partial n}\right)\Phi^2_{\boldsymbol{k}'}(t')\ . \tag{5.5}$$

First the integration of Fourier space was done - starting with the polar angle φ, followed by the integral with respect to k - before the time integration was done. The dimensionless integral $\mathcal{I}(t)$ was evaluated for the same shear rates and packing fractions as the $\delta S_{\boldsymbol{q}}^{\mathrm{aniso}}(\dot\gamma)$ (see section 5.1.1), leading to the results shown in figure 5.3.

As can be seen $\delta S_q^{\mathrm{iso}}(\dot\gamma)$ is a rapidly decaying function, oscillating around its large-wavevector limit $\delta S_{q\to\infty}^{\mathrm{iso}}(\dot\gamma)$. This limit is almost independent of the shear rate for constant η and small $\dot\gamma$ but increases with densification at constant (small) shear rate (see the inset in figure 5.3); for $\epsilon = 13^{-3}$ and $\mathrm{Pe}_0 = 10^{-4}$ the limit was found to be at 1.5 %. The oscillations appear to be asymmetric around their zeros and are equally spaced by $\mathrm{d}q \approx q_{\mathrm{p}}$. This is expected, since $\delta S_q^{\mathrm{iso}}(\dot\gamma)$ is dominated by the sum of the equilibrium structure factor and its derivative with respect to n. Thus the main peak occurs also at $q \approx q_{\mathrm{p}}$, the position of the primary peak of S_q.

Figure 5.3 shows the magnitude of the distortion depending smoothly on the shear rate and growing with Pe_0. But for low shear rates ($\mathrm{Pe}_0 = 10^{-4}$) a strong dependence on the packing fraction is visible: in the fluid states (corresponding to the linear response regime) the distortion is up to a decade smaller, compared to the shear-melted states deeper in the glass. The discontinuity at the glass transition can also be seen, because $\delta S_q^{\mathrm{iso}}(\dot\gamma)$ goes to zero for vanishing shear rate for $\epsilon < 0$ and remains finite in the glassy state for $\dot\gamma \to 0$; this is particularly visible for the zero-wavevector limit in figure 5.3(b).

However, the positions of extrema and zeros are not affected neither by shear nor by densification. Since the primary maximum of $\delta S_q^{\mathrm{iso}}(\dot\gamma)$ lies almost exactly on $q = q_{\mathrm{p}}$ - in combination with the first minimum and the corresponding root lying slightly below q_{p} - the isotropic distortion sharpens the primary peak of S_0 and increases it. $\delta S_q^{\mathrm{iso}}(\dot\gamma)$ has a shoulder (growing with η) at the low-q wing of its second peak $q \lesssim q_4$, which slightly broadens the lower slope of the second peak of the equilibrium structure - its peak in general is steeper. This holds less for the following peaks at larger q but the effect is still perceptible. All equilibrium peaks

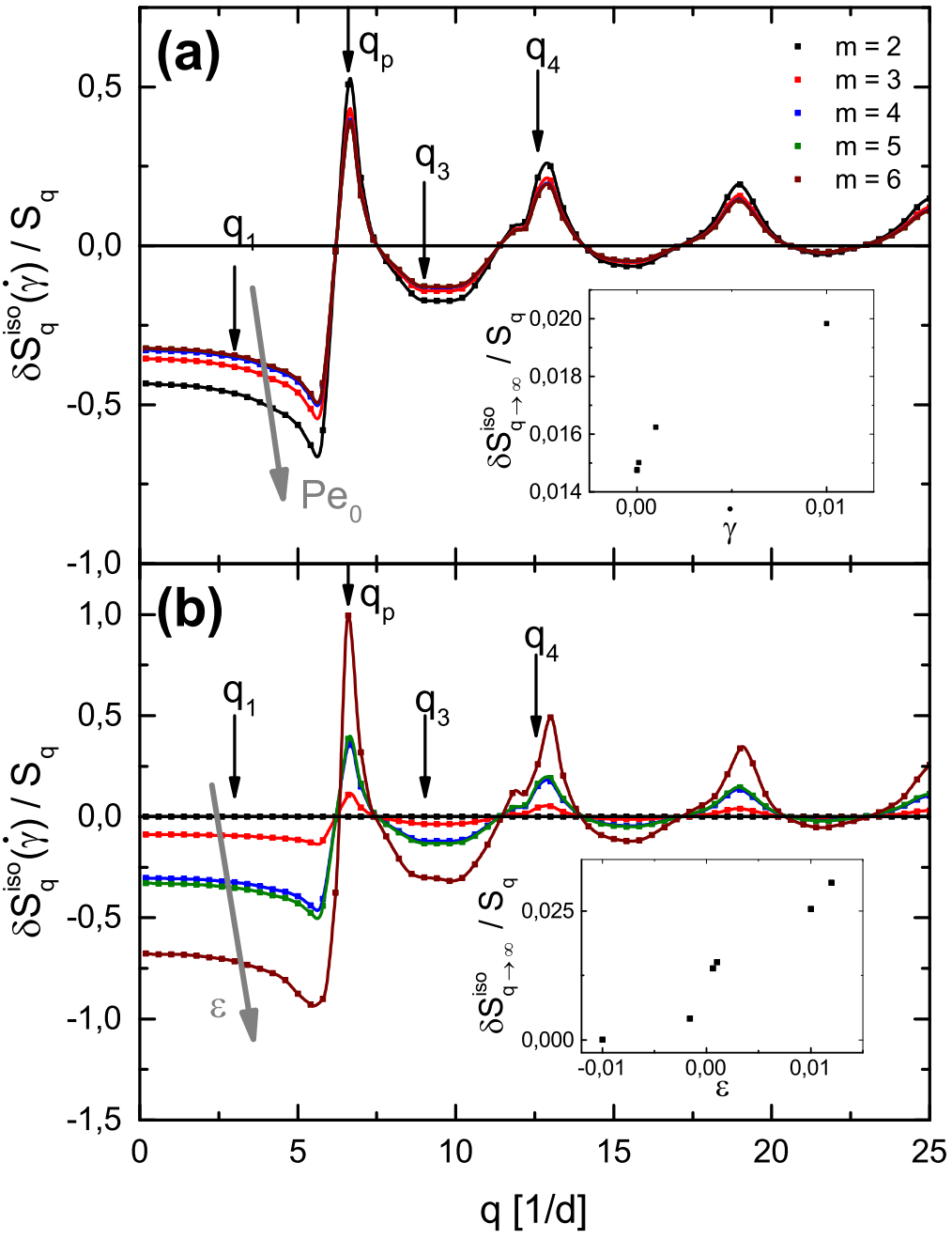

Figure 5.3.: Normalised isotropic structural distortion $\delta S_q^{\mathrm{iso}}(\dot{\gamma})/S_q$. **(a)**: different Péclet numbers $\mathrm{Pe}_0 = 10^{-m}$ with $m \in \{2,3,4,5,6\}$ as indicated for a separation parameter $\epsilon = 10^{-3}$. **(b)**: different separation parameters $\epsilon = -10^{-2}$ (black), $-1.6 \cdot 10^{-3}$ (red), $6.3 \cdot 10^{-4}$ (blue), 10^{-3} (green) and 10^{-2} (brown) for a Péclet number $\mathrm{Pe}_0 = 10^{-4}$; the distinguished wavevectors are $q_1 \approx 3$, $q_{\mathrm{p}} \approx 6.6$, $q_3 \approx 9$ and $q_4 \approx 12.6$. The insets show the corresponding normalised large wavevector limits.

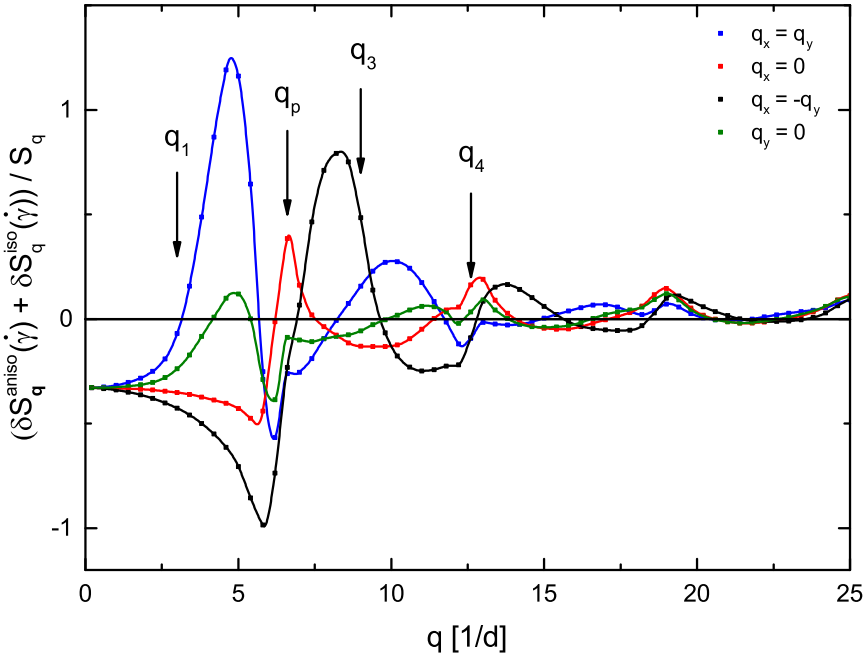

Figure 5.4.: Radial cuts through the normalised structural distortion $\delta S^{\text{aniso}}_{\boldsymbol{q}}(\dot\gamma) + \delta S^{\text{iso}}_{q}(\dot\gamma)/S_q$ in the four characteristic directions, as indicated, for $\epsilon = 10^{-3}$ and $\text{Pe}_0 = 10^{-4}$; the distinguished wavevectors are $q_1 \approx 3$, $q_\text{p} \approx 6.6$, $q_3 \approx 9$ and $q_4 \approx 12.6$.

are slightly shifted by approximately $0.3/d$ to larger wavevectors, which reflects a weak isotropic compression of the particles. The peak-sharpening (like $\delta S^{\text{aniso}}_{\boldsymbol{q}}(\dot\gamma)$ along the compressional axis) indicates additionally an increased mesoscale order of the colloids, which also is isotropic and caused by shear-induced flow.

5.1.3. Superposition

Combining the anisotropic and the isotropic distortion of the equilibrium structure generally leads to the qualitative aspects discussed above - as can be seen by comparison of figure 5.4 and figure 5.1. First and foremost the isotropic distortion decreases the effect of $S_{\boldsymbol{q}}(\dot\gamma)$ on the amplitude along the extensional axis (by approximately 25%) and increases the short range order in the direction perpendicular to the flow, where $\delta S^{\text{aniso}}_{\boldsymbol{q}}(\dot\gamma)$ does not contribute.

In [HPF07] an expansion was found for $S_{\boldsymbol{q}}(\dot\gamma)$ up to quadratic order in shear rate with regular coefficients containing the quiescent density correlators $\Phi_q(t)$ from

MCT [HPF07; Fuc10]:

$$S_q(\dot\gamma) = S_q + \dot\gamma \left(\frac{q_x q_y}{q} S'_q \int_0^\infty \mathrm{d}t \Phi_q^2(t) \right) + \mathcal{O}(\mathrm{Pe}_0^2) \; . \tag{5.6}$$

This expansion identifies the dressed Péclet (or Weissenberg) number $\mathrm{Pe} = \dot\gamma\tau$, with the α-relaxation time τ, being the small parameter of the expansion and predicts a distortion of the structure perpendicular to the flow in second order of $\dot\gamma$, rather than in linear order [HPF07]. But this expansion contains an error in quadratic order [Fuc10], and leads therefore to almost contrary results for the isotropic part in comparison to the ones obtained in this observations. There it shifts the main peak of $S_{\boldsymbol{q}}(\dot\gamma)$ to smaller wavevectors and the shape seems like the inverse of the results for the isotropic distortion in this elaboration.

5.2. Transient Evolution

Since the distorted structure and the stress tensor are connected via equation (6.2), there are major similarities in their transient behaviour. Many aspects regarding the overshoot will also be found in the discussion of $\boldsymbol{\sigma}(\dot\gamma)$ in the next chapter.

The integral in (5.4) shows qualitative differences according to three different time intervals and exhibits an overshoot[1], which increases with densification. The range of the evolution of the time integral occurring in (3.15) and (3.14) is mainly given by the transient density correlator, which is the origin for the time-depending behaviour of $\mathcal{I}(t)$ in the beginning and for large times. For small times $t \lesssim 0.01/\dot\gamma$, where the decay of $\Phi_{\boldsymbol{q}}(t)$ is caused by Brownian motion, the correlator (and therefore the hole integrand) is almost isotropic (as discussed in section 4.2). An exception holds for a dominating anisotropy that is given by the odd sinus function; thus the integration over angle gives nearly zero for small times. For the time interval of the first relaxation ($\dot\gamma t < 0.01$), the integral is expected to vary almost linear with time. When t comes in the regime of the final (α-) relaxation ($0.01 < \dot\gamma t < 1$), major anisotropies in the correlator causes the integral to grow strongly with time until it reaches a maximum absolute value $\mathcal{I}^{\max}$ for $\dot\gamma t \approx 0.1$, as can be seen in figure 5.5.

Since the $\Phi_{\boldsymbol{q}}(t)$ decays to zero for $\dot\gamma t \gtrsim 1$, $\mathcal{I}(t)$ reaches a plateau $|\mathcal{I}^{\lim}| < \mathcal{I}^{\max}$ for large times (corresponding to the stationary state).

The overshoot for times $0.4 \lesssim \dot\gamma t \lesssim 1$ has its seeds in the product $P_k(t) \equiv -S'_k(\partial S_{k(-t)}/\partial n)$, which behaves similar to $S'_k S'_{k(-t)}$ that was found in [Zau+08] to be crucial for the stress overshoot discussed in the next section. Figure 6.2 reveals that for $\dot\gamma t \gtrsim 0.4$ $P_k(t)$ exhibits negative regions growing with time. This causes the decay of $|\mathcal{I}(t)|$ after reaching its maximum value. This decay is suppressed by the decay of the correlator for $\dot\gamma t \gtrsim 1$, which then leads to the stationary value.

[1] Note: This is actually an undershoot, since the integral $\mathcal{I}(t)$ takes negative values. The denomination *overshoot* takes account of the complete isotropic distortion $\delta S_q^{\mathrm{iso}}(\dot\gamma)$ which is positive for large areas.

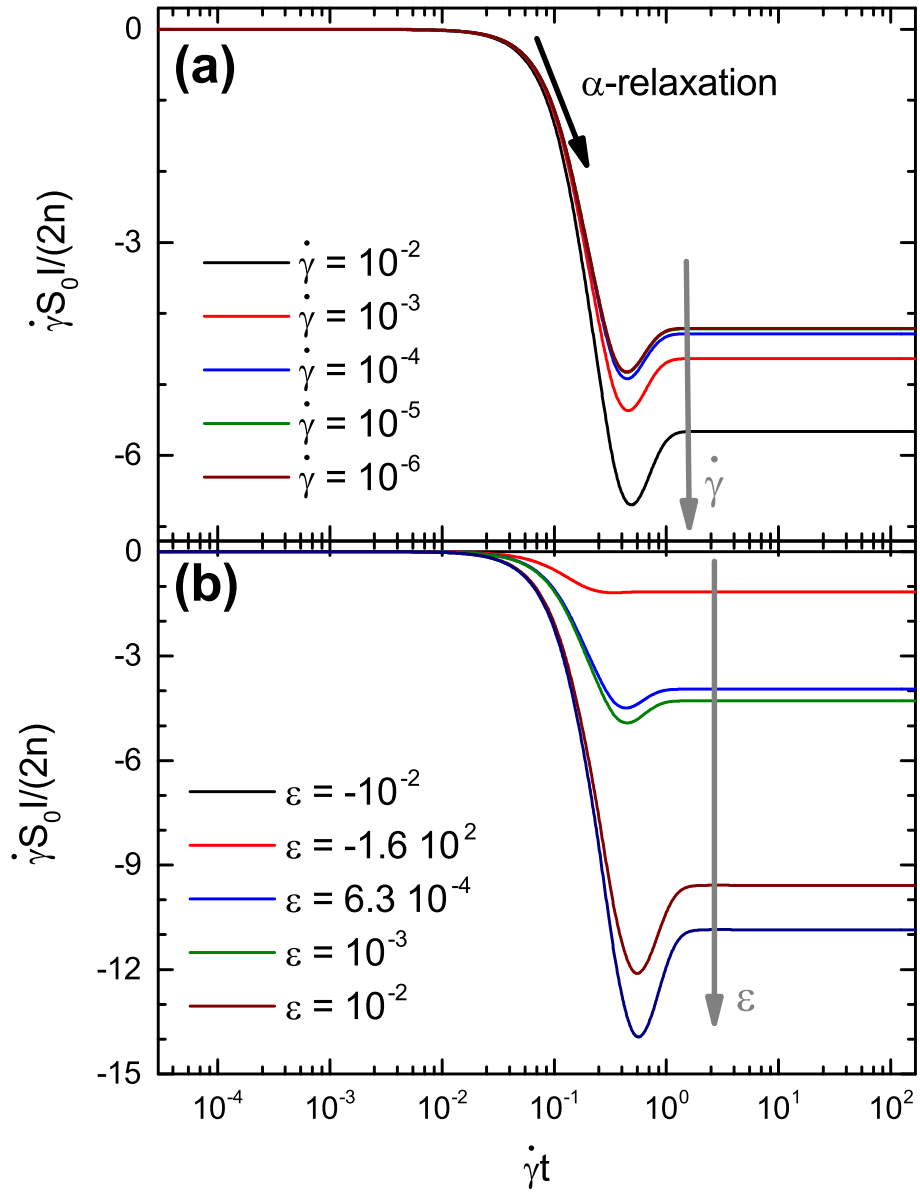

Figure 5.5.: Time-dependence of the isotropic integral $\dot\gamma S_0 \mathcal{I}(t)/2n$; **(a)**: different Péclet numbers $\mathrm{Pe}_0 = 10^{-m}$ with $m \in \{2,3,4,5,6\}$ (from top to bottom) for a separation parameter $\epsilon = 10^{-3}$. **(b)**: different separation parameter $\epsilon = -10^{-2}$, $-1.6 \cdot 10^{-3}$, $6.3 \cdot 10^{-4}$, 10^{-3} and 10^{-2} (from top to bottom) for a Péclet number $\mathrm{Pe}_0 = 10^{-4}$.

This behaviour can also be found in the stress-strain curves related to the solid-like elastic response, suddenly dominated by irreversible structural changes, which will be discussed in the next section.

As discussed in the context of the stationary values of $\delta S_q^{\mathrm{iso}}(\dot{\gamma})$, $\mathcal{I}(t)$ depends smoothly on the shear rate in the glass. This holds for the height of the overshoot $\Delta \equiv \left|\mathcal{I}^{\max} - \mathcal{I}^{\lim}\right|$, too. However, Δ depends sensitively on the packing fraction and the distance to the glass transition. In the glassy state it becomes very small while approaching η_{c} and almost disappears in the linear response regime in the fluid ($\epsilon = -10^{-2}$ and $\mathrm{Pe}_0 = 10^{-4}$; see figure 5.5).

6. Distorted Stress Tensor

Using the results obtained for the distorted structure the components of the stress tensor were calculated for a glassy system ($\epsilon = 10^{-3}$) under different shear rates; in this chapter the results are presented and discussed.

In [BCF12] a relation between the stress tensor and the distorted microstructure is given by[1]

$$\boldsymbol{\sigma}^{\text{aniso}}(\dot\gamma) \approx \frac{1}{2}\int \frac{\mathrm{d}^2k}{(2\pi)^2}\frac{\boldsymbol{kk}}{k}\frac{S_k'}{S_k^2}\left(S_k + \delta S_{\boldsymbol{k}}^{\text{aniso}}(\dot\gamma)\right) \ , \tag{6.1}$$

in which the isotropic distortion $\delta S_q^{\text{iso}}(\dot\gamma)$ was neglected. For the shear stress this is equivalent to the formulation in (3.8) which can be proofed by inserting the distorted structure from (3.14).

In the following sections the components of $\boldsymbol{\sigma}(\dot\gamma)$ will be discussed taking explicitly account on the effect of $\delta S_q^{\text{iso}}(\dot\gamma)$ on the stress tensor

$$\boldsymbol{\sigma}(\dot\gamma) = \boldsymbol{\sigma}^{\text{eq}} + \delta\boldsymbol{\sigma}^{\text{aniso}}(\dot\gamma) + \delta\boldsymbol{\sigma}^{\text{iso}} \tag{6.2}$$

with

$$\boldsymbol{\sigma}^{\text{eq}} = \frac{1}{2}\int \frac{\mathrm{d}^2k}{(2\pi)^2}\frac{\boldsymbol{kk}}{k}\frac{S_k'}{S_k} \ , \tag{6.3}$$

$$\delta\boldsymbol{\sigma}^{\text{aniso}}(\dot\gamma) \approx \frac{1}{2}\int \frac{\mathrm{d}^2k}{(2\pi)^2}\frac{\boldsymbol{kk}}{k}\frac{S_k'}{S_k^2}\delta S_{\boldsymbol{k}}^{\text{aniso}}(\dot\gamma) \ , \tag{6.4}$$

$$\delta\boldsymbol{\sigma}^{\text{iso}}(\dot\gamma) \approx \frac{1}{2}\int \frac{\mathrm{d}^2k}{(2\pi)^2}\frac{\boldsymbol{kk}}{k}\frac{S_k'}{S_k^2}\delta S_k^{\text{iso}}(\dot\gamma) \ . \tag{6.5}$$

6.1. Transversal Stress

The shear stress

$$\sigma_{xy}(\dot\gamma) = \sigma_{xy}^{\text{aniso}}(\dot\gamma) + \frac{1}{8\pi^2}\int_0^\infty \mathrm{d}k k^2 \frac{S_k'}{S_k^2}\delta S_k^{\text{iso}}(\dot\gamma)\cdot \underbrace{\int_0^{2\pi}\mathrm{d}\varphi \sin 2\varphi}_{=0} \tag{6.6}$$

is not affected by the isotropic distortion (nor by the equilibrium structure), since the isotropy causes the integral over φ to vanish and therefore $\delta\sigma_{xy}^{\text{iso}}(\dot\gamma)$ to disappear. In fig. 6.1 stress-strain curves (which are obtained from (6.6) for $\sigma_{xy}(\dot\gamma)$) are shown

[1] By comparing the expressions in [FC09] and [BCF12] for the macroscopic stationary stress a minus sign was found to be missing in equations (71) and (139) in [BCF12].

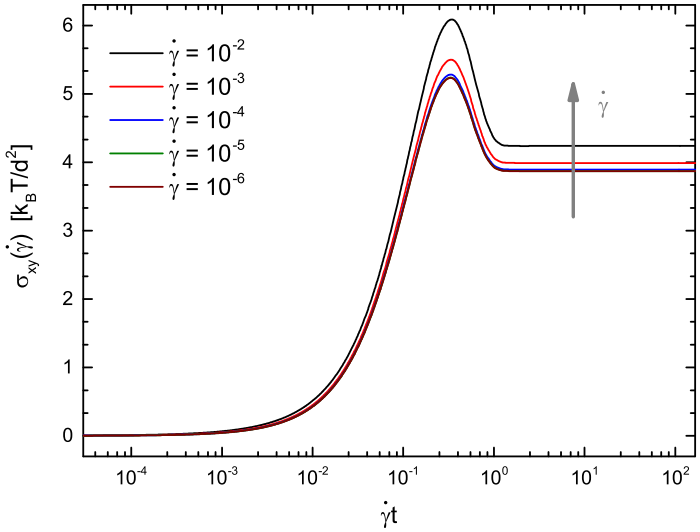

Figure 6.1.: Shear stress $\sigma_{xy}(\dot\gamma)$ for different Péclet numbers as indicated for a separation parameter $\epsilon = 10^{-3}$.

for different shear rates, where the accumulated strain is defined as $\gamma = \dot\gamma t$. The qualitative shape for constant $\dot\gamma$ is essentially dividable in three major sections, as also the transient behaviour of $\delta S_q^{\mathrm{iso}}(\dot\gamma)$ is:

For small strains $\gamma \lesssim 0.1$ $\sigma_{xy}(\dot\gamma)$ increases almost linearly, reflecting an elastic response of the system, similarly to a solid. Detailed observations - done in [Zau+08] - found a power law $\sigma_{xy}(\dot\gamma) \propto \gamma^x$ with $x < 1$ caused by the non-linear behaviour of the generalised shear modulus $g(t, \dot\gamma)$. This captures the effect of shear-thinning in the elastic regime for small strains [Zau+08],[Hen+09]. As can be seen in figure 6.1 the shear stress depends only less on $\dot\gamma$ for $\gamma \lesssim 0.1$.

Like the distorted structure the shear stress also performs an overshoot for $0.1 \lesssim \gamma \lesssim 1$, i.e. the elastic response continuing until the shear stress reaches its maximum $\sigma_{xy}^{\max}(\dot\gamma)$ for $\gamma \approx 0.1$ followed by a quick decay towards the asymptotic value. $\sigma_{xy}^{\max}(\dot\gamma)$ increases with the shear rate and shifts a little bit to higher strains, which can be found in figure 6.1. The origin of the overshoot, $S'_k S'_{k(-t)}$ in equation (3.8), was identified in [Zau+08]. As apparent in figure 6.2 this product shows negative regions in consequence of a growing de-phasing of the two derivatives with increasing strain. Since S'_k shows its largest amplitude around q_{p} and depends strongly on the shape of the primary peak in S_k, densification pronounces the overshoot [Zau+08]. For higher packing fraction the first peak in the equilibrium structure is steeper than for smaller η and thus the negative region in $S'_k S'_{k(-t)}$ increases with η. By remembering the definition of the shear modulus in (3.8) it appears that the behaviour of $S'_k S'_{k(-t)}$ causes a negative undershoot in $g(t, \dot\gamma)$ as function of time. Because of this the stress overshoot can be related to the fact that the shear modulus - in principle a

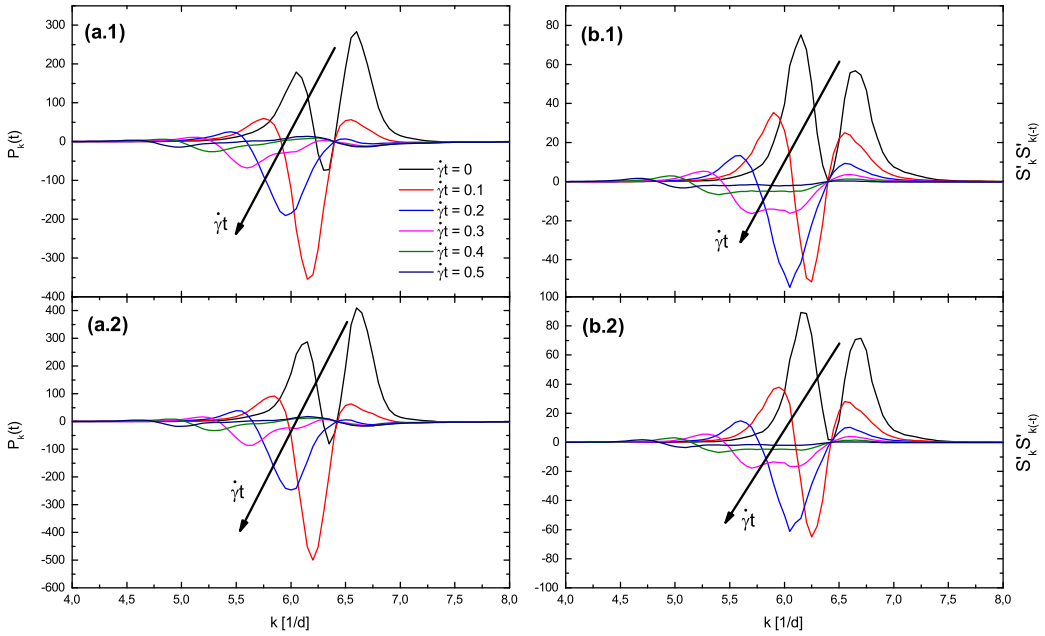

Figure 6.2.: Wavevector dependence of the Products that causes the overshoot in $\delta S_q^{\mathrm{iso}}(\dot{\gamma})$ and $\sigma_{xy}(\dot{\gamma})$ for two different separation parameter and different strains (as indicated). **(a)**: product $P_k(t)$, which occurs in $\mathcal{I}(t)$. **(b)**: product $S'_k S'_{k(-t)}$ from $\sigma_{xy}(\dot{\gamma})$.

stress autocorrelation function - takes negative values for times with $0.1 \lesssim \dot{\gamma}t \lesssim 1$, representing a stress over-relaxation or rather backscattering of stresses [Zau+08]. In [Zau+08] this was also linked with the diffusion coefficient and the mean square displacement, such that the overshoot in $\sigma_{xy}(\dot{\gamma})$ is connected to a super-diffusive behaviour of the colloidal particles [Zau+08].

For strains $\gamma \gtrsim 1$ the shear stress reaches a plateau $\sigma_{xy}(\dot{\gamma}, t \to \infty) \equiv \sigma^{\infty}(\dot{\gamma})$ and is constant thereafter. Since the evolution of the distorted structure (which depends mainly on the transient correlators) dictates the evolution of the stress with increasing strain (or time respectively), the latter depends on $\Phi_{\boldsymbol{q}}(t)$ in the same way as $\delta S^{\text{aniso}}_{\boldsymbol{q}}(\dot{\gamma})$ - this connection is explicit visible in (3.8). Thus, $\sigma_{xy}(\dot{\gamma})$ reaches its asymptotic value $\sigma^{\infty}(\dot{\gamma}) < \sigma^{\max}_{xy}(\dot{\gamma})$ after the transient correlator is decayed to zero by the α-relaxation. This suppresses the negative contributions from the product $S'_k S'_{(-t)}$ and thus brings the shear modulus to zero for long times [Zau+08]. The asymptotic values $\sigma^{\infty}(\dot{\gamma})$ form the flow curves when plotted in dependence of the shear rate. The plateau implies, that the system is kept flowing by shear, and increases with shear rate, which means that faster flow induces more internal stress [Zau+08].

Recalling the master function of the transient density correlator and the dynamic yield contribution to the distorted structure factor, a dynamical yield stress $\sigma^{+}_{xy}(\epsilon) \equiv \sigma_{xy}(\dot{\gamma} \to 0, \epsilon)$ can be predicted ([FC09],[Hen+09]) that characterises the transition from a shear-thinning fluid to a yielding glass: In the fluid state ($\epsilon < 0$) $\sigma^{+}_{xy}(\epsilon)$ remains zero in contrast to its finite value in a shear-melted glassy state ($\epsilon > 0$); Directly at the transition it is discontinuous [Hen+09].

In [Hen+09] and [Zau+08] the MCT-ITT results for the shear stress were found to capture qualitatively the results of molecular dynamic simulations and experimental data (obtained by confocal microscopy) but with significant quantitative differences. Especially the stress overshoot is underestimated by the theory [Zau+08].

6.2. Normal Stress

In contrast to $\sigma_{xy}(\dot{\gamma})$ the normal stress is affected by the isotropic structural distortion:

$$\sigma_{\alpha\alpha}(\dot{\gamma}) = \sigma^{\text{aniso}}_{\alpha\alpha}(\dot{\gamma}) + \frac{1}{8\pi^2}\int_0^{\infty} \mathrm{d}k k^2 \frac{S'_k}{S_k^2}\delta S^{\text{iso}}_k(\dot{\gamma}) \int_0^{2\pi} \mathrm{d}\varphi \begin{cases} \cos^2\varphi, & \alpha = x \\ \sin^2\varphi, & \alpha = y \end{cases} , \tag{6.7}$$

where $\delta\sigma^{\text{iso}}_{xy}(\dot{\gamma}) \neq 0$. Since both integrals with respect to φ give the value π, the normal stress components in the steady state differ from $\sigma^{\text{aniso}}_{\alpha\alpha}$ in a constant $c_\sigma(\dot{\gamma})$ only, which depends on the shear rate:

$$\sigma_{\alpha\alpha}(\dot{\gamma}) = \sigma^{\text{aniso}}_{\alpha\alpha}(\dot{\gamma}) + c_\sigma(\dot{\gamma}) \, , \tag{6.8}$$

$$c_\sigma(\dot{\gamma}) = \frac{1}{8\pi}\int_0^{\infty} \mathrm{d}k k^2 \frac{S'_k}{S_k^2}\delta S^{\text{iso}}_k(\dot{\gamma}) \, . \tag{6.9}$$

Note that nevertheless c_σ contains the full transient behaviour of the isotropic structural distortion $\delta S_q^{\mathrm{iso}}(\dot\gamma)$ discussed in section 5.1.2 - including the overshoot of $\mathcal{I}(t)$. Thus, the transient behaviour of $\sigma_{\alpha\alpha}(\dot\gamma)$ is also expected to change when $\delta S_q^{\mathrm{iso}}(\dot\gamma)$ is taken into account.

Figure 6.3 shows the normal stress components as a function of the accumulated strain γ - calculated with and without the isotropic structural distortion. Taking a closer look at the pressure $p^{\mathrm{aniso}}(\dot\gamma) \equiv -1/2(\sigma_{xx}^{\mathrm{aniso}}(\dot\gamma) + \sigma_{yy}^{\mathrm{aniso}}(\dot\gamma))$, which is given by

$$p^{\mathrm{aniso}}(\dot\gamma) = -\frac{1}{16\pi^2}\int_0^\infty \mathrm{d}k \int_0^{2\pi} \mathrm{d}\varphi k^2 \underbrace{\left(\cos^2\varphi + \sin^2\varphi\right)}_{=1} \frac{S_k'}{S_k^2}\left(S_k + \delta S_{\boldsymbol{k}}^{\mathrm{aniso}}(\dot\gamma)\right) \quad (6.10)$$

and shown in figure 6.3 reveals that the normal components of the stress tensor exhibit an overshoot on average already without the isotropic contribution, as the shear stress does, too. This overshoot is inherited from the anisotropic structural distortion $\delta S_{\boldsymbol{q}}^{\mathrm{aniso}}(\dot\gamma)$ and has the same origin as the one in the shear stress: the product $S_k' S_{k(-t)}'$ concealed in $S_k' \delta S_{\boldsymbol{q}}^{\mathrm{aniso}}(\dot\gamma)$. In the single components $\sigma_{\alpha\alpha}^{\mathrm{aniso}}(\dot\gamma)$ this product is modulated by the cosine or the sine, accordingly. The cosine cancels all contributions from the y-direction diagonal to the flow (where $\delta S_{\boldsymbol{q}}^{\mathrm{aniso}}(\dot\gamma)$ is zero anyway) and emphasises the x-direction, hence $\sigma_{xx}^{\mathrm{aniso}}(\dot\gamma)$ shows a pronounced overshoot. On the other hand $\sigma_{yy}^{\mathrm{aniso}}(\dot\gamma)$ is an almost monotonous function, because all contributions from the flow direction are cancelled by the sine function.

If the isotropic structural distortion is taken into account, this superimposes the transient behaviour of $\sigma_{\alpha\alpha}^{\mathrm{aniso}}(\dot\gamma)$ and $\delta S_q^{\mathrm{iso}}(\dot\gamma)$. The overshoot of the stress tensor components is cancelled by the undershoot of $c_\sigma(\dot\gamma)$, as can be seen in figure 6.3. The latter is generated by the overshoot of the time integral in $\delta S_q^{\mathrm{iso}}(\dot\gamma)$, whereupon the k-integration causes a negative sign, since the product $-P_k(0)$ appears in $c_\sigma(\dot\gamma)$ and has a major negative region (cf. figure 6.2).

The stationary values of the normal stress components are heavily decreased[2] with increasing shear rate. This means in terms of the deviatoric stress

$$\delta\boldsymbol{\sigma} = \delta\boldsymbol{\sigma}^{\mathrm{aniso}} + \delta\boldsymbol{\sigma}^{\mathrm{iso}} \quad (6.11)$$

that $\delta\boldsymbol{\sigma}^{\mathrm{iso}}$ causes a change of sign from $\delta\sigma_{\alpha\alpha}^{\mathrm{aniso}} > 0$ to $\delta\sigma_{\alpha\alpha} < 0$.

Since the pressure is the negative arithmetic average of the normal stress components, it is affected in the same way by the isotropic part of $S_{\boldsymbol{q}}(\dot\gamma)$. The isotropic distortion switches the sign of the undershoot of $p^{\mathrm{aniso}}(\dot\gamma)$ and enlarges its magnitude. This is equivalent to a change of sign of the deviatoric pressure

$$\delta p(\dot\gamma) = \delta p^{\mathrm{aniso}}(\dot\gamma) + \delta p^{\mathrm{iso}}(\dot\gamma) = -\frac{1}{2}\left(\delta\sigma_{xx}(\dot\gamma) + \delta\sigma_{yy}(\dot\gamma)\right) \quad (6.12)$$

from $\delta p^{\mathrm{aniso}}(\dot\gamma) < 0$ to $\delta p(\dot\gamma) > 0$ if $\delta S_q^{\mathrm{iso}}(\dot\gamma)$ is no longer neglected. Note that the complete transient properties are present the deviatoric quantities, whereas

[2] That means increased absolute values.

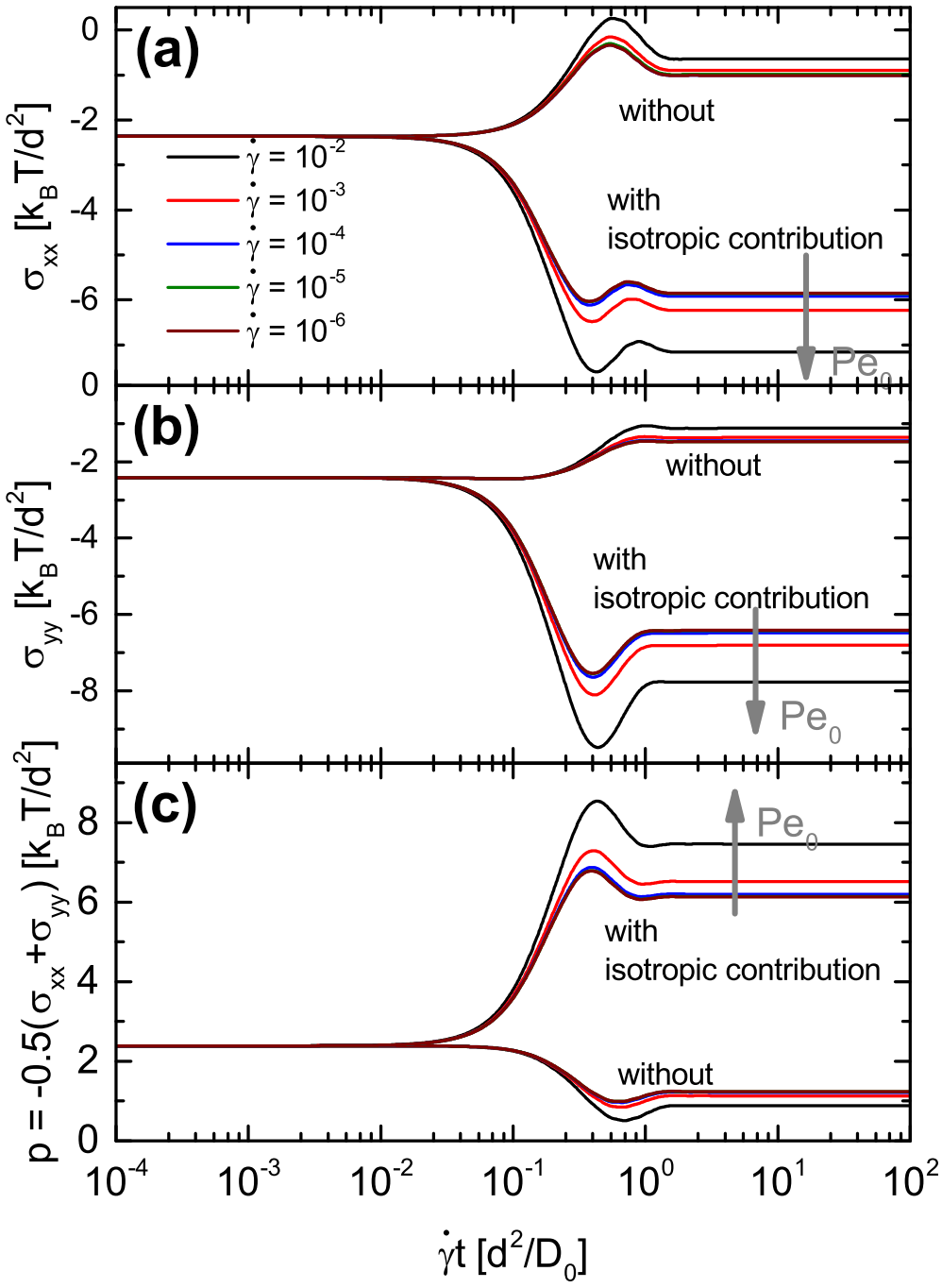

Figure 6.3.: Normal stress components of the stress tensor components and pressure as function of the accumulated strain γ, calculated with and without the isotropic contribution of the structural distortion for different Péclet numbers as indicated and a separation parameter $\epsilon = 10^{-3}$.

the equilibrium quantities are constants for all times. Hence the overshoot in the pressure is kept inside $\delta p(\dot{\gamma})$.

The superposition of the overshoots of $\delta\sigma_{\alpha\alpha}^{\text{aniso}}(\dot{\gamma})$ and the undershoot of $c_\sigma(\dot{\gamma})$ causes a tiny oscillation before the pressure reaches its asymptotic value for large times. This asymptotic (or stationary) values of the pressure are shifted by the same constants as $\sigma_{\alpha\alpha}^{\text{aniso}}(\dot{\gamma})$ for different shear rates, but in the inverse direction.

7. Local Order and Pair Structure

In [Ama+15] the effect of shear on the microscopic structure and the stress was analysed in real space with the help of pair correlation functions. The results from molecular dynamic simulations, Brownian dynamic (BD) simulations and data from confocal microscopy were compared with the predictions of the MCT-ITT formalism, whereupon the isotropic structural distortion was neglected in the theory.

The general connection between the pair correlation function $g(\boldsymbol{r})$ and the structure factor $S(\boldsymbol{k})$ is given by the Fourier transformation [HM06]:

$$ng(\boldsymbol{r}) = \int \frac{\mathrm{d}^3k}{(2\pi)^3} \left(S(\boldsymbol{k}) - 1\right) e^{i\boldsymbol{k}\boldsymbol{r}} \,. \tag{7.1}$$

By transforming the shear depending distorted structure factor $S_{\boldsymbol{k}}(\dot{\gamma})$ one can obtain the shear distorted pair correlation function

$$ng(\boldsymbol{r}, \dot{\gamma}) = g_\mathrm{e}(r) + \delta g^\mathrm{aniso}(\boldsymbol{r}, \dot{\gamma}) + \delta g^\mathrm{iso}(\boldsymbol{r}, \dot{\gamma}) \tag{7.2}$$

with its components within two dimensional MCT given by

$$g_\mathrm{e}(r) = \int \frac{\mathrm{d}^2k}{(2\pi)^2} \left(S_k - 1\right) e^{i\boldsymbol{k}\boldsymbol{r}} \,, \tag{7.3}$$

$$\delta g^\mathrm{aniso}(\boldsymbol{r}, \dot{\gamma}) \approx \int \frac{\mathrm{d}^2k}{(2\pi)^2} \delta S^\mathrm{aniso}_{\boldsymbol{k}}(\dot{\gamma}) e^{i\boldsymbol{k}\boldsymbol{r}} \,, \tag{7.4}$$

$$\delta g^\mathrm{iso}(\boldsymbol{r}, \dot{\gamma}) \approx \int \frac{\mathrm{d}^2k}{(2\pi)^2} \delta S^\mathrm{iso}_{k}(\dot{\gamma}) e^{i\boldsymbol{k}\boldsymbol{r}} \,. \tag{7.5}$$

By using the projection on the spherical harmonics Y_{lm} the distortion of the pair structure can be expanded in single modes

$$\delta g_{lm}(r, \dot{\gamma}) = \int\int \mathrm{d}\vartheta \mathrm{d}\varphi \; \delta g(\boldsymbol{r}, \dot{\gamma}) Y^*_{lm}(\vartheta, \varphi) \tag{7.6}$$

containing the symmetries of the corresponding angular momenta, which are indicated by l and m [Ama+15]. By this proceeding quadrupolar deformations of the angular dependence of $g(\boldsymbol{r}, \dot{\gamma})$ were found in [Ama+15], which are corresponding to an angular momentum $l = 2$. These are dominant for small strains ($\gamma < 0.1$) in the elastic response regime, where the shear stress increases almost linearly. For higher strains, when the overshoots occur, the pair structure is dominated by a deformation that shows hexadecopular symmetry ($l = 4$). This could be related to irreversible deformations due to plastic flow and cage breaking [Ama+15].

These results were found in good agreement with the simulation data, but major differences between BD simulations and the predictions of MCT occurred, concerning the isotropic deformation modes[1] $\delta g_{00}(r, \dot{\gamma})$, which occur near the contact of the particles.

The BD simulation was found $\delta g_{00}(r, \dot{\gamma})$ to be monotonously increasing with strain at contact, following the dependence of the simulation's deviatoric pressure $\delta p(\dot{\gamma})$ [Ama+15]. On the contrary MCT-ITT without $\delta S_q^{\mathrm{iso}}(\dot{\gamma})$ predicts a further decreasing negative distortion of the pair structure at the contact value. This is replicated by the results for $\delta \boldsymbol{\sigma}^{\mathrm{aniso}}(\dot{\gamma})$, which are calculated in the context of this elaboration and discussed in section 6.2, because MCT provides the following relation between the deviatoric stress tensor and the pair correlation function:

$$\delta \boldsymbol{\sigma}(\dot{\gamma}) = -\frac{n}{2} \int \mathrm{d}^2 r \delta g(\boldsymbol{r}, \dot{\gamma}) \boldsymbol{\nabla}(\boldsymbol{r} c(r)) \; . \tag{7.7}$$

In section 6.2 $\delta \boldsymbol{\sigma}^{\mathrm{aniso}}(\dot{\gamma})$ was found to be positive and to exhibit an overshoot at strains $\gamma \approx 0.1$. Because the integral in (7.7) is dominated by the nearest neighbour contributions at the scale of a single particle diameter [Ama+15], $\delta g^{\mathrm{aniso}}(\boldsymbol{r}, \dot{\gamma})$ is therefore expected to be negative and to vary non-monotonously with the strain.

This discrepancy can made void to some extent by including the full distorted structure with its isotropic contribution. This causes a change of the sign whereby $\delta \boldsymbol{\sigma}(\dot{\gamma})$ becomes negative, as detailed in section 6.2. This in turn changes the sign of $\delta g(\boldsymbol{r}, \dot{\gamma})$, which then increases with strain on the contact value - although it performs an overshoot (because $\delta p(\dot{\gamma})$ does).

Thus, isotropic deformations of the local pair correlations do not contain the right qualitative behaviour that was found in BD simulations, albeit the isotropic structural distortion $\delta S_q^{\mathrm{iso}}(\dot{\gamma})$ leads to a first correction of the deformation mode $\delta g_{00}(r)$ at the contact value.

[1] Because $Y_{00}(\vartheta, \varphi) = 1/\sqrt{4\pi}$, $\delta g_{00}(r, \dot{\gamma})$ is merely the azimuthally average of $\delta g(\boldsymbol{r}, \dot{\gamma})$ [Ama+15].

8. Conclusion

Within the presented frame in chapters 2 and 3 the full distorted structure factor of a dense colloidal dispersion under shear was calculated for different shear rates and packing fraction close to the glass-transition. For the first time, the isotropic contribution $\delta S_q^{\mathrm{iso}}(\dot{\gamma})$ was included in the calculation, which was found to represent an isotropic compression of the particles and to show the same qualitative transient behaviour as the shear stress $\sigma_{xy}(\dot{\gamma})$. The origin of the overshoot has found to be the product $P_k(t)$, which arises from the thermodynamic relation in [Bax64]. While the transversal stress is not affected itself, the isotropic contribution leads to a quite different behaviour of the normal stress components that shifts the sign of the deviatoric pressure

$$\delta\sigma_{\alpha\alpha}^{\mathrm{aniso}}(\dot{\gamma}) > 0 \;\Rightarrow\; \delta p^{\mathrm{aniso}}(\dot{\gamma}) < 0 \,, \tag{8.1}$$

$$\delta\sigma_{\alpha\alpha}(\dot{\gamma}) < 0 \;\Rightarrow\; \delta p(\dot{\gamma}) > 0 \,. \tag{8.2}$$

The connection of the stress tensor with the contact values of the pair correlation by equation (7.7) provides the prediction, that this change of sign will cause a correction for the isotropic deformation mode $\delta g_{00}(r)$ of the distorted pair correlation function, which then would be in agreement with the BD simulation results from [Ama+15], pertaining to the sign of the deformation mode.

However, qualitative differences in the transient behaviour remain, because the overshoot of $\delta p(\dot{\gamma})$, which is caused by the one of $\delta S_q^{\mathrm{iso}}(\dot{\gamma})$, is not captured by the simulations, where the isotropic deformation increases monotonous with the strain. Therefore it would be interesting to go back to real space and investigate the concrete effects $\delta S_q^{\mathrm{iso}}(\dot{\gamma})$ has on the pair correlations and their isotropic deformation modes, to check this predictions. Maybe a deeper look in the derivation of the approximated distorted structure (3.15) can be interesting, in order to find the principle origin of the deviating behaviour (i.e. the overshoot and the non-zero limit for large wavevectors) and enhance the approximation.

A. Numerical Details

In this chapter the numerical topics of this elaboration are presented in detail. This includes testing the used algorithm and important aspects of the several calculations. Furthermore the discretisation is motivated.

A.1. Testing the Algorithm

Numerical integration was performed using the composed trapezoidal rule for both the integration over Fourier space and over time, in order to find a compromise between performance and accuracy.

First the implemented algorithm was tested with several polynomials before a full three-dimensional integration was executed of an analytical integrable function, that captures the main qualitative behaviour of the integrand in (3.15). In these tests the implemented algorithm matches the exact solutions with a relative deviation of 0.5% on average within the chosen discretisation (cf. section 4.3).

By calculating the integral $\mathcal{I}(t)$ in the isotropic distortion of the structure factor for different step-sizes in time the convergence of the algorithm was studied. The same calculation was also done by using the composed rectangle method with both upper sums and lower sums in order to give first rough bounds of the result: Since the integrand is an (almost) monotonously increasing function of time in the interval where the largest contributions are expected ($t \in [10^2, 10^3]$, before $S_k' \partial S_{k(-t)}/\partial n$ becomes negative), lower sums should almost slightly overestimate the exact solution whereas the other should almost underestimate it[1]. This behaviour could be verified, as shown in figure A.1: The results of the rectangle method frame the outcome of the trapezoidal rule and all three methods converge into a joint limit value if the step size is diminished. Also the order of the convergence agrees with the theory for both the linear converging rectangle method and the implemented trapezoidal rule, which is known to be convergent of second order. When fitted with a power function $\tilde{\mathcal{I}(t)} = a + \Delta t^p$ for the trapezoidal method the power $p \approx 2.4$ was found, whereas the rectangle rules are found to converge with order $p \approx 0.8$ for the upper sums and with $p \approx 1.3$ for the lower sums.

Another possibility for testing the algorithm appears because of the equivalence of equations (3.8) and (6.6). The difference in calculating $\sigma_{xy}(\dot{\gamma})$ directly from the transient dynamics and by using the distorted structure is equivalent to inverting

[1] Note that in $\mathcal{I}(t)$ the integration over k and φ gives negative values for times $t \lesssim 10^{-3}$, and thus the remaining integrand is a negative function of t - viz. increasing means a decreasing absolute value.

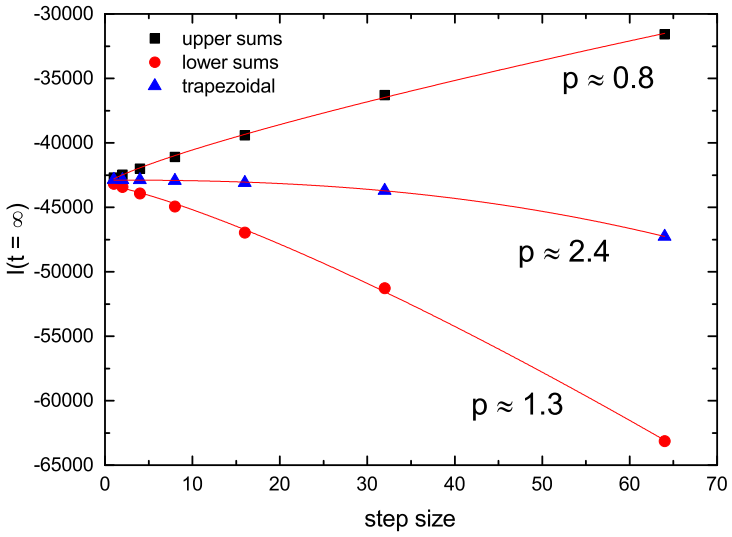

Figure A.1.: Results of the two different rectangle methods (with upper and lower sums) and the trapezoidal rule (as indicated) for the integral $\mathcal{I}(t = \infty)$ in the isotropic distortion of the stationary structure factor; including fits with the power function $\tilde{\mathcal{I}}(t) = a + \Delta t^p$ and the obtained numerical orders of convergence p.

the sequence in which the Fourier and the time integration are performed. By this way a deviation from approx. 3% could be found, which is probably caused by rounding errors.

A.2. Special Numerical Tasks

The input quantity $\Phi_{\boldsymbol{q}}(t)$ from [Kb] is given on the same grid, which arises from the spherical discretisation used for the numerical calculations described in section 4. However, the equilibrium structure lies on a much finer grid along the radial axes and is given for several packing fractions η. This was beneficial, since it had to be interpolated in order to be able to evaluate S_q and its derivations for arbitrary wavevectors and packings. The derivations with respect to q and to the density were then obtained by differentiation of the interpolating function.

For the calculation of $\delta S^{\text{aniso}}_{\boldsymbol{q}}$ interpolation was also needed for the transient correlator, since in the integral $\Phi_{\boldsymbol{q}}(t)$ has to be evaluated at the advected wavevectors $\boldsymbol{q}(-t)$ which do not match the grid-points. Likewise the advected wavevectors leave the data range of $\Phi_{\boldsymbol{q}(-t)}(t)$ for large times, hence the interpolated correlators were set to zero for $q \geq 40$. This is bearable, because for small times, where the correlators might not be decayed completely at $q \geq 40$, the value of the integral remains very small in relation to later times $\dot{\gamma}t \gtrsim 10^{-2}$. In the last interval ($\dot{\gamma}t \gtrsim 1$) the correlators are decayed completely for larger wavevectors; hence the error by the

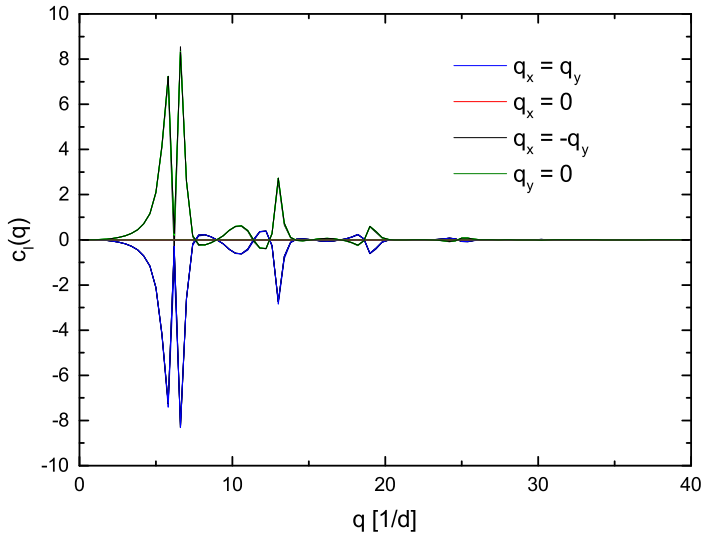

Figure A.2.: Wavevector dependence of the integrand $c_{\mathcal{I}}(k)$ of $\mathcal{I}(t)$ for $\dot{\gamma}t \approx 10^{-2}$ for the four characteristic directions, that are indicated in the picture.

cutoff is negligible.

To avoid interpolation of the correlators in the integral $\mathcal{I}(t)$ in the isotropic contribution, the two dimensional integration of the Fourier space was performed over the advected wavevectors $\boldsymbol{k}(-t) \equiv \boldsymbol{k}'$ instead of $\boldsymbol{k}$, using the transformation $\boldsymbol{k} = \boldsymbol{k}' - \dot{\gamma}tk_x\hat{\boldsymbol{y}}$ with $k_x = k'_x$. By going to polar coordinates via $\boldsymbol{k}' = k' \left(\cos\varphi', \sin\varphi'\right)^{\mathrm{T}}$ the magnitude of the wavevector $\boldsymbol{k}$ is then given by

$$k = k'\sqrt{1 - \dot{\gamma}t \sin 2\varphi' + (\dot{\gamma}t \cos\varphi')^2} \; . \tag{A.1}$$

In figure A.2 the k-dependence of the integrand $c_{\mathcal{I}}(k)$ of $\mathcal{I}(t)$ is shown for four characteristic directions. For small times $\dot{\gamma}t \lesssim 10^{-4}$ the integrand is not declined as it reaches the boundary of the discretisation. But hence it is dividable in a nearly isotropic part that is modulated by the odd sinus function, the integration of the angle gives almost zero in this time interval. For $\dot{\gamma}t \gtrsim 10^{-2}$ where the increasing anisotropies causes non-zero values of the φ-integration the integrand is completely decayed before it reaches the cutoff $q = 39.8$.

A.3. Discretisation

All calculations were done with the spherical discretisation of the Fourier space which was introduced in section 4.3. Its advantage is that several directions can be obtained for constant q, which is not easy with a Cartesian grid. This is useful concerning the crucial anisotropies in the transient correlators and the distorted

structure. Additionally the spherical grid, as a cobweb, intrinsically emphasises the angular space at small wavevectors by small spacing whereas the angular resolution for larger q gets coarser. This weighting is in agreement with the requirements in this calculations, because the major anisotropies occur for $qd \lesssim 15$. Thus, by a spherical grid a higher resolution of the most relevant area is possibly than per a Cartesian discretisation with the same count of lattice points - without the need for missing larger wavevectors.

Bibliography

References

[Ama+15] C. P. Amann et al. "Hexadecupolar modes as signature of yielding in metallic and colloidal glasses". unpublished. 2015.

[Bax64] R. J. Baxter. "Direct Correlation Functions and Their Derivatives with Respect to Particle Density". In: *The Journal of Chemical Physics* 41.2 (1964). DOI: http://dx.doi.org/10.1063/1.1725907.

[Bay+07] M. Bayer et al. "Dynamic glass transition in two dimensions". In: *Physical Review E* 76.1 (2007). DOI: 10.1103/PhysRevE.76.011508.

[BCF12] J. M. Brader, M. E. Cates, and M. Fuchs. "First-principles constitutive equation for suspension rheology". In: *Physical Review E* 86.2 (2012). DOI: 10.1103/PhysRevE.86.021403.

[FC05] M. Fuchs and M. E. Cates. "Integration through transients for Brownian particles under steady shear". In: *Journal of Physics: Condensed Matter* 17.20 (2005). DOI: 10.1088/0953-8984/17/20/003.

[FC09] M. Fuchs and M. E. Cates. "A mode coupling theory for Brownian particles in homogeneous steady shear flow". In: *Journal of Rheology* 53.4 (2009). DOI: 10.1122/1.3119084.

[For75] D. Forster, ed. *Hydrodynamic fluctuations, broken symmetry, and correlation functions*. Vol. 47. W. A. Benjamin, Inc. (Frontiers in Physics), 1975. ISBN: 978-0201410495.

[Fuc10] M. Fuchs. "Nonlinear Rheological Properties of Dense Colloidal Dispersions Close to a Glass Transition Under Steady Shear". In: *High Solid Dispersions*. Ed. by Michel Cloitre. Vol. 236. Advances in Polymer Science. Springer Berlin Heidelberg, 2010, pp. 55–115. ISBN: 978-3-642-16381-4. DOI: 10.1007/12_2009_30.

[Hen+09] O. Henrich et al. "Hard discs under steady shear: comparison of Brownian dynamics simulations and mode coupling theory". In: *Philosophical Transactions of the Royal Society of London* 367.1909 (2009). DOI: 10.1098/rsta.2009.0191.

[HM06] J.-P. Hansen and I. R. McDonald. "Chapter 4 - Distribution-function Theories". In: *Theory of Simple Liquids (Third Edition)*. Ed. by J.-P. Hansen and I. R. McDonald. Burlington: Academic Press, 2006, pp. 78 –108. ISBN: 978-0-12-370535-8. DOI: 10.1016/B978-012370535-8/50006-9.

[HPF07] O. Henrich, O. Pfeifroth, and M. Fuchs. "Nonequilibrium structure of concentrated colloidal fluids under steady shear : leading-order response". In: *Jornal of Physics: Condensed Matter* 19 (2007). DOI: 10.1088/0953-8984/19/20/205132.

[Kb] Courtesy M. Krüger and J.M. Brader.

[KWF11] M. Krüger, F. Weysser, and M. Fuchs. "Tagged-particle motion in glassy systems under shear : comparison of mode coupling theory and Brownian Dynamics simulations". In: *The European Physical Journal E* 34.9 (2011). DOI: 10.1140/epje/i2011-11088-5.

[Zau+08] J. Zausch et al. "From equilibrium to steady state: the transient dynamics of colloidal liquids under shear". In: *Journal of Physics: Condensed Matter* 20.40 (2008). DOI: 10.1088/0953-8984/20/40/404210.

Further Information

[BH03] J.-L. Barrat and J.-P. Hansen. *Basic Concepts for Simple and Complex Liquids*. Cambridge University Press, 2003. ISBN: 9780511606533.

[Kaw70] K. Kawasaki. "Kinetic equations and time correlation functions of critical fluctuations". In: *Annals of Physics* 61.1 (1970). DOI: 10.1016/0003-4916(70)9037

[KGF09] M. Krüger, H. Günter, and M. Fuchs. "Fluctuation Dissipation Relations in Stationary States of Interacting Brownian Particles under Shear". In: *Physical review letters* 102 (2009). DOI: 10.1103IPhysRevLett.102.135701